Study and Characterization of a Metal Matrix Composite Reinforced with Tantalum Carbide-TaC

Leiliane Alves de Oliveira[1], Uílame Umbelino Gomes[2], Carlson Pereira Souza[3], Sérgio Renato da Silva Soares[4]

[1, 2, 3] Graduate Program in Materials Science and Engineering, Federal University of Rio Grande do Norte – UFRN. Natal, RN, Brazil

[4] Degree in Mechanical Engineering. Federal University of Mato Grosso - UFMT. Rondonopolis, MT, Brazil

leilianealves@gmail.com; uilame.umbelino@pq.cnpq.br; carlson@ufrnet.br; sergeva2004@yahoo.com.br

Abstract

Steel is an alloy EUROFER promising for use in nuclear reactors, or in applications where the material is subjected to temperatures up to 550°C due to their lower creep resistance under. One way to increase this property, so that the steel work at higher temperatures it is necessary to prevent sliding of its grain boundaries. Factors that influence this slip contours are the morphology of the grains, the angle and speed of the grain boundaries. This speed can be decreased in the presence of a dispersed phase in the material, provided it is fine and homogeneously distributed. In this context, this paper presents the development of a new material metal matrix composite (MMC) which has as starting materials as stainless steel EUROFER 97, and two different kinds of tantalum carbide-TaC, one with average crystallite sizes 13.78 nm synthesized in UFRN and another with 40.66 nm supplied by Aldrich. In order to improve the mechanical properties of metal matrix was added by powder metallurgy, nano-sized particles of the two types of TaC. This paper discusses the effect of dispersion of carbides in the microstructure of sintered parts. Pure steel powders with the addition of 3% TaC UFRN and 3% TaC commercial respectively were ground for 5 hours in the planetary mill. Each of the resultant particulate samples were cold compacted under a uniaxial pressure of 600MPa in a cylindrical die 5 mm in diameter. Subsequently, the compressed were sintered in a vacuum oven at a temperature of 1250°C with an increment of 20°C and 10°C per minute and maintained at these isotherms for 60 minutes. The distribution, size and dispersion of steel and composite particles were determined by X-ray diffraction, laser particle size and scanning electron microscopy(SEM). The structures of the sintered bodies were observed by optical microscopy(OM) and scanning electron microscopy(SEM).

Keywords

EUROFER97; TaC; Powder Metallurgy; MMC

Introduction

Studies show that the steels can have their properties improved with the addition of particulate oxides or metal carbides dispersed in the metal matrix. Mechanical strength is among these properties, with which reinforcement particles dispersed in the matrix may increase the steel armor working temperature since it works as a mechanism that prevents dislocation movements and, consequently, there is an improvement in the deformation strength, preventing crack propagation and increasing fatigue strength.

EUROFER steel (9cr-1W) is very promising and can be used in power generation turbines, pressure vessels, nuclear reactors or applications in which the material is submitted to temperatures between 250 and 450°C. A way to improve the steel properties, so that it works at higher temperatures or becomes more stable, is to add second-phase particles to the matrix. These particles can be in the form of oxides, carbides, nitrides and even as some solid solutions where chemicals are added to the material. In this context, the aim of this study was to present an improvement in the mechanical properties of Eurofer steel reinforced with nano-sized tantalum carbide particles (TaC).

The State of Rio Grande do Norte is a major producer of refractory metals (W, Ta, Nb), ceramic minerals (diatomite, kaolin, feldspar, mica, barite, clays, etc) and other minerals containing rare earth and semi -precious stones.

2226-4523/15/02 040-5 © 2015 DEStech Publications, Inc.
doi:10.12783/ijmsci.2015.0502.02

However, this natural richness that places the state among the top five mineral producers in the country has not reversed into progress and development for the region, mainly due to the lack of technological aggregation to local raw materials.

In this context, a new sintered material was obtained by powder metallurgy technique (P/M) from high-energy ball milling of the nanostructured ferritic / martensitic stainless steel (EUROFER97) and tantalum carbide (TACs) particulate material.

Powder metallurgy (P/M) is a route that can be used to produce metal components of alloy steel reinforced with oxides and carbides to obtain materials with better properties and dimensional control [7]. Powder metallurgy is an economically viable route for the processing of complex metal parts with high finishing quality and tolerance when compared to conventional techniques [8]. In Metal Matrix Composites (MMCs), a component often acts as a matrix in which the reinforcement is dispersed. Reinforcements may be in the form of particles, wires, short fibers or continuous fibers.

High-energy ball milling (RBM) started in 1966 by an industrial need for the production of super alloys based on nickel and iron (dispersed oxides) for applications in the aerospace industry [9]. Therefore, this type of milling is an alternative to the production of powders to be used in compaction and sintering steps.

The main aim of this work was the development and characterization of a new Metal Matrix Composite material – MMC, able to have good densification and high hardness. Thus, a study on the development and characterization of this MMC, having as matrix a ferritic / martensitic stainless steel (EUROFER97) containing tantalum carbide powders as reinforcement with nanometric dimensions, consolidated via solid phase sintering, was carried out. Carbides were chosen because they are stable, do not react with the metal matrix and have high melting point and high hardness.

Experimental Procedure

Starting from a bar-shaped material, after characterizing the starting material, machining was performed and the chip was removed, and from this, the grinding process started. Firstly, the grinding of the pure steel was performed, and then, steel with the addition of 3% TaC-UFRN and 3% TaC- commercial. Powders were milled for 5 hours in a high-energy planetary mill. The resulting particulate composite powders were characterized for particle size, x-ray Diffraction and Scanning Electron Microscopy (SEM), being then cold compacted under uniaxial pressure of 600 MPa into a cylindrical matrix of 5 mm in diameter. Subsequently, samples were sintered in a vacuum oven at temperature of 1250°C isotherm for 60 minutes. Sintered samples were cooled to room temperature. The structures of sintered specimens were observed by optical microscopy (OM) and Scanning Electron Microscopy and analyzed by microhardness tests.

Results

Figure 1 shows peaks characteristic of each tantalum carbide (TaC), TAC-UFRN and TAC-Aldrich and Table 1 shows the crystallite size and microdeformation of powders through Ritveld analysis.

Figure 2 shows the microstructure of EUROFER97 stainless steel as received in the shape of bar (Fig2) with martensitic / ferritic microstructure, as can be seen in the Figure. Hardness measured and the mean value was 333.2HV.

Figure 3 shows the particle size profiles of pure steel powder of composite particles with TaC UFRN and that supplied by Aldrich, all ground for 5 hours in high-energy planetary mill. Large variation in particle size and a modal graph can be observed. This behavior may be related to the state of particles agglomeration, since it was not possible to disperse particles thoroughly with soap or by ultrasound. The average sizes found by this technique were 28.21 μm for pure powder, 29.09 μm for steel with TaC-UFRN and 35.06 μm for steel with TaC-commercial.

Figure 4 shows the X-ray patterns of pure Eurofer, Eurofer with TaC-UFRN (ETU) and with TaC-Aldrich (ETC). In the first case, only peaks associated with the Fe with CCC structure were observed, which is the same structure of the ferrite phase. The same Fe peaks are observed in the other diffractogram, but with the presence of characteristic

TAC peaks (4B and 4C). Comparing Figures 4b and 4c, the peak of Fe in the CCC structure is more intense in Figure 4c than in particulate composite of steel with TaC-UFRN (4B), both results using the same processing.

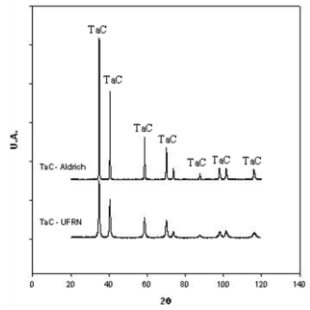

Powders	CS (nm)	Md (%)
TaC Sigma	40.66	$1.02x10^{-4}$
TaC UFRN	13.78	$1.56x10^{-3}$
Obs.: CS = Crystallite size; Md = microdeformation		

FIGURE 1. AND TABLE 1 STANDARD EXPERIMENTAL X-RAY DIFFRACTION OF TANTALUM CARBIDE SIGMA ALDRICH AND UFRN - RESULTS OF THE CRYSTALLITE SIZE AND MICRODEFORMATION OBTAINED FOR TWO DIFFERENT TANTALUM CARBIDES (OLIVEIRA ET AL, 2007).

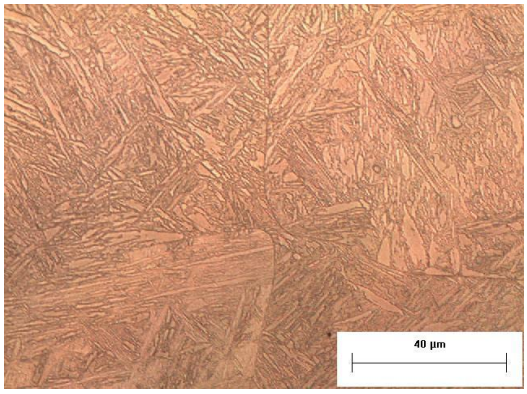

FIGURE 2. MICROGRAPHS (OM - 500X), A) OF STEEL BAR EUROFER ATTACKED WITH VILELA (2%).

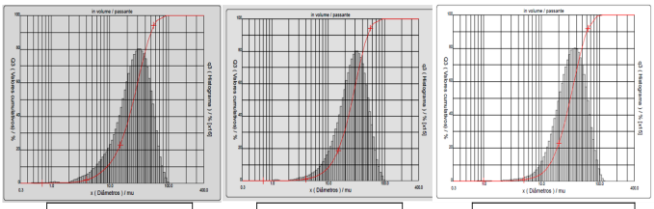

PURE EUROFER97 (5hs)	
Diameter a 10%	8.95 µm
Diameter a 50%	25.51 µm
Diameter a 90%	50.70 µm
Diameter Medium	28.21 µm

Steel with TaC UFRN (5hs)	
Diameter a 10%	10.92 µm
Diameter a 50%	26.59 µm
Diameter a 90%	50.34 µm
Diameter Medium	29.09 µm

Steel with TaC commercial (5hs)	
Diameter a 10%	13.65 µm
Diameter a 50%	31.57 µm
Diameter a 90%	60.19 µm
Diameter Medium	35.06 µm

FIGURE 3. RESULTS OF LASER PARTICLE SIZE OF EUROFER 97 STEEL, STEEL WITH TAC-UFRN AND STEEL WITH TAC-COMMERCIAL SIMULTANEOUSLY MILLED FOR 5 HOURS.

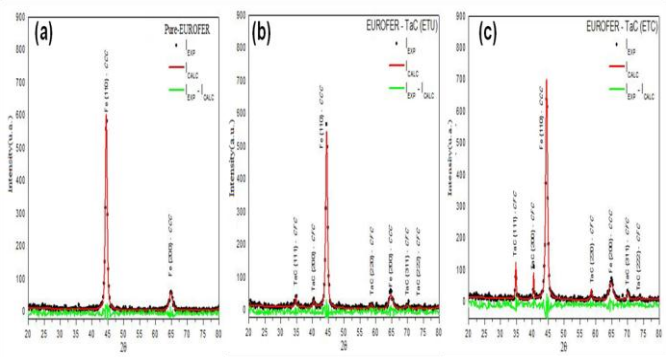

FIGURE 4. PURE EUROFER97 DIFFRACTOGRAM (A) EUROFER97 WITH TAC-UFRN (B), AND EUROFER97 WITH TAC-COMMERCIAL (C).

Figure 5 shows the micrographs of pure Eurofer 97 steel particles (FIGURE5a), steel with TaC-UFRN (FIGURE 5b) and steel with TaC-Aldrich (FIGURE 5c), each milled for 5 hours with magnification of 600x and bar size of 50 m. It was observed that the particle size was drastically reduced, but there is still a substantial difference in particle size. The morphological analysis of Eurofer 97 shows irregular particle shapes and size distribution and rough surfaces, as can be seen in Figure 5 (a). Figure 5 (b) shows a finer morphology of steel particles, but still not uniform, and TaC-UFRN particles indicated by the arrow can be visualized dispersed in the metal matrix. In Figure 5c, it was observed that there is a similarity between the particle size of the pure steel powder (FIGURE5a) and the particle size of steel powder with TaC-Aldrich (FIGURE 5c), as well as TaC particles indicated by the arrow dispersed in the steel particles. Figure 6 shows the micrograph (OM) of samples sintered at temperature of 1250°C for 60 minutes. According to the arrangement of samples, the following images were obtained, micrographs of pure sintered steel (Figure 6a), steel with TaC-UFRN (Figure 6b) and sintered steel with TaC-commercial (Figure 6c). Figure 6a shows the size of grain contours and the presence of two phases, ferrite (lighter part) and martensitic (darker part), Figure 6b shows sintered ETU with the presence of many pores, compared with the other two sintered samples under the same conditions, but pores in segmented shapes in particles and also in rounded shape, indicating sintering at stage shifting from intermediate stage to the final stage. A microstructure with diffuse phases was observed, with light and dark parts. Figure 6c shows densified samples and grain contours with small and regular shapes and sizes, but with the presence of a single phase, characteristic of ferritic phase, which can influence the mechanical properties of the material.

SEM images (Figure 7) show the morphology of pure sintered EUROFER97steel (FIGURE 7a), the dispersion TaC-UFRN particle in the steel matrix (FIGURE 7b) and dispersion of TaC- commercial particles in the steel matrix (FIGURE 7c). Figure 4a shows a microstructure with small and rounded pores, indicating the end of the sintering

stage. Figure 7b shows a porous microstructure with TaC-UFRN particles dispersed within the contours of the pore, thereby hindering the pore closing and preventing the densification of the material. Unlike what occurs in composites reinforced with TaC-Aldrich, this sample has a densified microstructure, with a dispersion of TaC particles (white part) randomly dispersed in the matrix (gray part).

Table 2 shows the large difference in microhardness values between pure steel (EP) and steel with UFRN-TaC (ETU) in comparison with steel with TaC-commercial (ETC). This difference is associated with the dispersion of coarse particles and / or fine particles of the reinforcement added to the metal matrix. Another issue would be regarding the phases of steels, which in the case of sintered sample of pure EUROFER steel (EP), it can be associated with the type of phase transformation that in this case, did not occur, maintaining its ferritic / martensitic structure, but in the case of composite steel with TaC-commercial, ferritic phase prevailed, and thus a smaller microhardness value compared with the other samples was obtained. In ETU sample, in addition to the presence of fine dispersed particles and / or embedded into the metal matrix of the EUROFER steel, the phases (ferritic / martensitic) of the original material may remain in the composite.

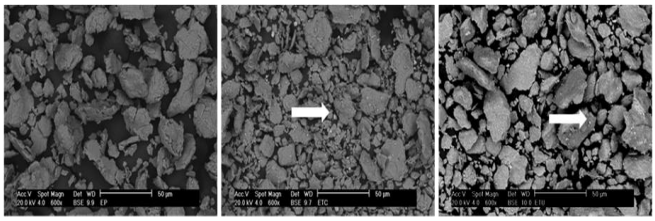

FIGURE 5. (SEM - 600X) PARTICULATE POWDERS GROUND FOR 5 HOURS IN PLANETARY MILL, PURE STEEL EUROFER POWDER (A) STEEL WITH TAC-UFRN, (B) STEEL WITH TAC-COMMERCIAL (C).

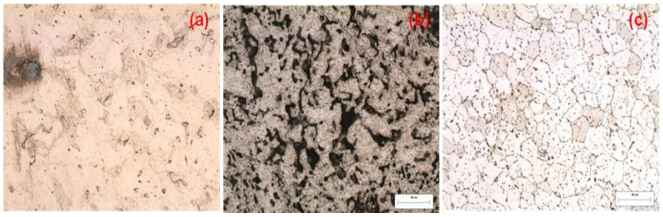

FIGURE 6. MICROGRAPHS (OM - 500X) OF SAMPLES SINTERED AT 1250°C FOR 60 MINUTES, (A) PURE EUROFER (EP), (B) EUROFER WITH TAC-UFRN (ETU) AND (C) EUROFER WITH TAC-COMMERCIAL (ETC).

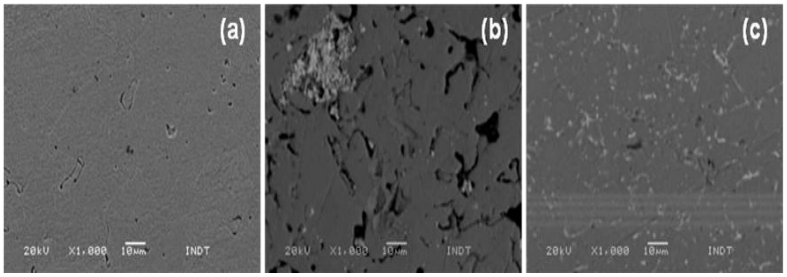

FIGURE 7. MICROGRAPHS (SEM - 1000X) OF SINTERED AT 1250°C FOR 60 MINUTES; (A) PURE EUROFER (EP), (B) EUROFER WITH TAC-UFRN (ETU) AND (C) EUROFER WITH TAC-COMMERCIAL (ETC).

TABLE 2. HARDNESS RESULTS OF COMPOSITE MILLED OR 5 HOURS, SINTERED AT TEMPERATURE OF 1250°C FOR 60MINUTES.

Samples	Microhardness (HV)
EP	636.8 ± 35.6
ETU	700.6 ± 17.0
ETC	191.2 ± 8.0

PE = Pure Eurofer; ETU = Eurofer + TaC-UFRN
and ETC = Eurofer + TaC-Commercial, supplied by Aldrich.

Conclusion

A new composite has been produced by powder metallurgy with considerable mechanical properties, even starting from a bar-shaped material. Powders were obtained by high-energy milling with reduced sizes as observed in the particle size analysis related to the starting material.

Tantalum carbide - TaC with strongly agglomerated nano-sized crystallites, forming particles smaller than those of EUROFER 97 steel particles were dispersed by grinding, remaining in compression among particles that compose the metallic matrix, thus obtaining a material with finer microstructure, smaller grain size and good mechanical properties.

Using the of X-ray diffraction technique of powders and sintered samples, it was possible to detect the presence of TaC and Fe-CCC components, reinforcement and elements of the metal matrix, respectively, used in this study.

SEM images show sintered samples of pure steel and steel composite with TaC-UFRN, where typical microstructures of sintered material were observed, with sintering stages ranging from: initial, intermediate the final. In addition, the dispersion of tantalum carbides in the metal matrix of EUROFER steel was observed.

Optical microscopy showed a change in grain size, as well as in the microstructure of different sintered materials. For samples added of TaC, the grain size decreased or remained stable, compared with pure steel. The sintering temperature of 1250°C provided high densification in composite reinforced with TaC supplied by Aldrich, but low hardness result, which may be related to a phase change, i.e., the steel became fully ferritic.

The powder metallurgy process was sufficient to improve the mechanical property of EUROFER steel, with a small difference between microhardness results between it and composite reinforced with UFRN-TaC. In the case of composite reinforced with TaC-commercial, there is a considerable difference, which can be related to the phase transformation and / or coarse particles compared with UFRN-TaC powder particles, which are thinner.

ACKNOWLEDGMENT

Acknowledgment at UFRN, PPGCEM, CAPES and CNPQ.

REFERENCES

[1] Lucon, E.; Leenaers, A., Vandermeulen, W.; Mechanical response of oxide dispersion strengthened (ODS) EUROFER97 after neutron irradiation at 300ºC. Fusion Engineering and Design, v. 82, p. 2438-2443, 2007.

[2] Cayron, C.; Rath, E.; Chu, I.; Launois, S. Microstructural evolution of Y2O3 and MgAl2O4 ODS EUROFER steels during their elaboration by mechanical milling and hot isostatic pressing. Journalof Nuclear Materials, v. 335, p. 83-102, 2004.

[3] Furukava, M., Sinteringof steel reinforced with dispersed nanometrics particules of niobium carbide – NbC. Doctoral Tesis, Federal University of Rio Grande do Norte – Natal, Brazil. 2007. In Portuguese.

[4] Oliveira, L. A., Sintering stud of 316L steel reinforced with 3% of Tantalum Carbide – TaC Master Tesis, Federal University of Rio Grande do Norte – Natal, Brazil. 2013. In Portuguese.

[5] Castro V., Leguey T., Munõz A., Monge M. A., Fernádez P., Lancha A. M., Pareja R., Mechanical dispersion of Y2O3 nanoparticles in steel EUROFER97: process and optimization. Journal of Nuclear Materials, v. 322, p. 228-234, 2003.

[6] Castro, V., Leguey T., Munõz A., Monge M. A., Fernádez P., Lancha A. M., Pareja R., Mechanical and microstructural behaviour of Y2O3 ODS EUROFER97. Journal of Nuclear Materials, v. 367-370, p. 196-201, 2007.

[7] Gomes, U. U., *Tecnologia dos Pós – Fundamentos e Aplicações* -. Brasil: UFRN, 1995.

[8] Gotoh, K., Masuda, H.; Higashitani, K. Powder Technology Handbook. Second Edition. ed. Nova York: Editora Marcel Dekker Inc., 1997.

[9] Suryanarayana, C.; Ivaniv, E.; Boldyrev, V. V., The science and technology of mechanical alloying. Materials Science and Engineering A, v. 304-306, p. 151-158, 2001.

[10] Cayron, C. Rath, E.; Chu, I.; Launois, S., Microstructural evolution of Y2O3 and MgAl2O4 ODS EUROFER steels during their elaboration by mechanical milling and hot isostatic pressing. Journal of Nuclear Materials, v. 335, p. 83-102, 2004.

[11] Souza, C. P.; Medeiros, F. F. P.; Gomes, U. U., Carbide Of obtaining In Tantalo nanostructured The Low Temperature from Precursor oxalate (NH4) 3 [Tao (C2O4) 3] .1,5h2o Reaction From Through Gas-Solid. (2005).

Nisin as an Antibacterial Substance in Active Packaging: 2. Use of Ethylene Methyl Acrylate and Co-Polyamide to Enhance Its Effectiveness

Gilad Reichenberg*[1], Amos Ophir[1], Yiftach Nir[1]

Plastics engineering department, Shenkar collage, 12 Anna Frank St. Ramat-Gan, Israel

*[1]gilad22z@yahoo.com; [2]amosophir@shenkar.ac.il; [3]yiftachnir@shenkar.ac.il

Abstract

This work deals with flexible thermoplastic films incorporating nisin for antibacterial active packaging purposes. A novel approach was used to gain control over nisin release profile from a thermoplastic film with the aim of enhancing nisin antibacterial efficiency. The release profile of nisin from active packaging to foodstuff is a key factor concerning the enhancement of its efficiency. In our last study, polymer blends of EVA and co-polyamide were used to control nisin migration from film to foodstuff simulant. In this part, EVA was replaced by EMA due to applicable reasons. Samples of 400μm thick were produced by using a laboratory twin screw compounder and a laboratory hot press (same as part 1). Release kinetics and antibacterial tests were done in order to characterize different target bacteria response to different migration profiles. Listeria ATCC 33090 was used as target bacteria. Nisin migration profile to foodstuff simulant was determined by Lowry's protocol. Osmotic pressure driven release mechanism appears to be the migration mechanism and diffusion kinetics was dominant.

Results show that polymer blend continues phase determines the diffusion coefficient. Furthermore, films were characterized for their elastic modulus properties as supplementary data. Elastic modulus and nisin concentration in foodstuff stimulant show an inverse proportion. It is concluded that this proportion is related to the formation of more surface area that is exposed for migration.

Keywords

Active Packaging; Antibacterial Film; Controlled Release; Nisaplin; Nisin; Polymer Blends

Introduction

One of the most relevant fields concerning bacterial contamination is daily consumed ready-to-eat foodstuffs. Food-borne pathogens are a growing concern worldwide because people are exposed to it on a daily basis. The World Health Organization (WHO) and the European Food Safety Authority (EFSA) report in recent years that there has been an increase in food-borne illnesses. Products that are animal origin such as milk, eggs and meat are especially a concern because they acquire the microflora from their environment. Animal origin foodstuffs have a history of more than 50% of total food-borne illnesses in the 1990's. Listria monocytogens and other pathogens are distributed in the environment and are parts of the microflora of humans. Food contamination can occur as a result of hygienic failures during the processing of packaged foodstuff [1].

Bacterial contamination occurs primarily at the surface of foodstuffs due to post processing handling. Attempts have been made to disinfect the surface of contaminated foodstuffs by using direct formulated antibacterial sprays or dips. This direct application had little effect due to antibacterial activity exhaustion [2].

Flexible polymer packaging is increasingly used for foodstuff packaging purposes as a physical barrier from the surroundings among other reasons. Active packaging is a sophisticated approach for the preservation of fresh foodstuffs, control over food-borne pathogens and extension of shelf life [3]. This sophisticated approach actively involves the foodstuff's polymeric packaging in the preservation of its content, besides being a physical barrier. The objective of an antibacterial active packaging is controlled over bacterial prosperity of non-sterile foodstuffs, maintaining the pasteurized stability for sterile foodstuffs and extended shelf life [4].

2226-4523/15/02 045-9 © 2015 DEStech Publications, Inc.
doi:10.12783/ijmsci.2015.0502.03

Nisin is a potent polypeptide bacteriocin produced by the lactic acid bacteria. Nisin is water soluble, exhibits greatest stability under acidic conditions and is known to inhibit the growth of gram-positive bacteria. It has been used by humans for decades and is considered safe for consumption [5] [6] [7] [8]. Controlling over the release kinetics of nisin is of essence. Its antibacterial effectiveness increases when controllation is released to the surface of foodstuff, and is compared with traditional nisin instant addition [9] [10] [11]. Release kinetics control technology is used in many fields particularly in drug delivery devices. One method of obtaining control over drug release kinetics is using polymer blends [12]. Each polymer has its own effect on drug release kinetics and by changing the ratio of the polymers in the blend – drug release kinetics control is achieved.

This work aims to study the enhancement of antibacterial effectiveness of nisin incorporated polymer blend films.

Experimental

Methodology

In order to obtain nisin incorporated polymer films that controls nisin release kinetics and possess antibacterial activity, suitable polymer components were selected according to thermal, rheological and hygroscopic properties:

Since nisin is susceptible to thermal conditions [7] [13], high processing temperature polymers were screened. Hygroscopic properties were of interest since nisin migration occurs on a liquid water medium basis.

Deionized Water (DI water) was used as a migration medium. In order to verify nisin migration from film to DI water, preliminary water swelling tests were done. Polymers that did not increase their water swelling extent as Nisaplin incorporation were screened. Preliminary bacterial tests determined that nisin antibacterial activity was retained in the determined processing conditions and that nisin migration occurred to DI water (data not shown).

This work has applicable purposes, therefore, films containing 4wt% of Nisaplin were of interest.

Materials

Two polymers were used as polymer matrix components: Elvaloy ac1820 supplied by Dupont (EMA). This ethylene methyl acrylate copolymer is designed for flexible packaging and complies with the rules and complies with the U.S food and drug administration regulations for use in contact with all types of food.

Some properties include: melting point of 92°C, 20% of methyl acrylate content, MFR = 8cm^3/10min (ASTM D1238) and density of 0.942 gr/cm^3.

Grilon CF 6 S was generously donated by EMS (PA). This Co-polyamide(6,12) is designed for packaging applications and complies with EU requirements and FDA regarding food contact. Some properties include: melting point of 130°C, MVR = 180cm^3/10min (ISO 1133) and density of 1.05gr/cm^3.

Nisaplin, supplied by Handary SA, Brussels, Belgium (Nis) is a commercial product. Nisaplin appearance is a light brown fine powder and is composed of 2.5wt% nisin, 95wt% sodium chloride and remains of milk solids asreported by the manufacturer.

Sample Preparation

Compound Preparation

EMA, PA and Nisaplin were compounded using a twin screw extruder (Prism, EuroLab). Screw speed was 250 RPM and temperature profile was 160°C for all five heating zones. Samples of 4wt% Nisaplin were produced for biological tests and samples of 12wt% Nisaplin for migration tests. Composition ratios are specified in table 1.

TABLE 1. SAMPLE COMPOSITIONS.

Sample notation	Matrix composition EMA/PA [wt%]	Nisaplin (Nisin) [wt%]
EMA/Nis4	100/0	4 (0.1)
EMA/PA-30/Nis4	70/30	4 (0.1)
EMA/PA-50/Nis4	50/50	4 (0.1)

EMA/PA-70/Nis4	30/70	4 (0.1)
PA/Nis4	0/100	4 (0.1)
EMA/Nis12	100/0	12 (0.3)
EMA/PA-30/Nis12	70/30	12 (0.3)
EMA/PA-50/Nis12	50/50	12 (0.3)
EMA/PA-70/Nis12	30/70	12 (0.3)
PA/Nis12	0/100	12 (0.3)

Film Prepartion

Films were prepared using a laboratory hot press and a rectangular shaped mold. The Laboratory press was heated to 160°C and samples were incubated for 5 minutes. Pressure of 15,000psi were applied for 10 seconds and the resulting film thickness was about 400μm.

Characterization

Thermal Analysis (DSC)

DSC (TA instruments, Q200) was used (temperature ramp of 10°C/min) in order to evaluate the degree of polymer blend interactions by monitoring the change of characteristic transition temperatures with composition.

In order to eliminate the thermal history, two runs were performed within a temperature range of (-40) – 200°C.

Scanning Electron Microscopy (SEM)

SEM (Aspex, explorer) was used in order to characterize polymer blend morphology and evaluation of Nisaplin responsing to water activity at the time nisin migration occurs. Samples were immersed for 24 hours in DI water in order to witness film state. Samples were let to dry, a cryogenic fracture was done and the cross section was examined. Samples were coated with a thin layer of gold and images were captured at a magnification of 750X.

Nisin Migration Profile

The effect of polymer blend composition on nisin migration profile to DI water was evaluated using migration cells at room temperature. Migration cells were composed of a glass cell equipped with a removable 60mm diameter lid. 10ml of DI water was introduced to the cell as migration medium. Nisaplin incorporated films were cut to fit the cell's lid. Each container was positioned so that DI water and film contact took place. Films were let to reach equilibrium for one hour. Sink conditions were verified [14]. At specific time intervals, water samples were taken and characterized for their nisin concentration by Lowry's protocol [15]. A U.V visible spectrophotometer (SHIMADZU, UV-1650PC) was used to evaluate the absorbance peak at 750nm. Nisaplin was used as standard. Samples were tested using triplicates.

Mechanical Properties

A tensile test was conducted in order to evaluate the influence of mechanical properties on the migration extent [16]. The tensile test was conducted, according to ASTM D882, at room temperature and samples were let to condition for more than 40 hours prior to the test. Test conditions were initial grip separation of 50mm and rate of grip separation was 500mm/min. Each result consists of five tests.

Antibacterial Activity

In order to evaluate the antibacterial activity of the films, a Gram-positive target bacteria (Listeria ATCC 33090) was used. Antibacterial activity tests were done at 50% nutritional broth (NB) at room temperature. Samples were tested using duplicates. Corresponding control films were tested and no significant influence on target bacteria was seen (data were not shown). Films containing 4wt% Nisaplin were tested, as noted earlier, due to an applicative approach and the high sensitivity of this test.

Results and Disscusion

Thermal Analysis (DSC)

A DSC diagram of EMA/PA blends is shown in figure 1. Melting temperatures of 130°C and 92°C can be seen for PA and EMA blends respectively. EMA/PA-70 sample does not show the EMA melting point, due to the existence of a Tcc peak at 78°C which is attributed to PA. The PA glass transition temperature shown is about 29°C. EMA glass transition temperature is not evident at this DSC diagram and not reported by the manufacturer. All EMA/PA blends show approximately these glass transition temperatures without any significant change with composition. It is concluded that no significant physical interactions exist in these blend compositions.

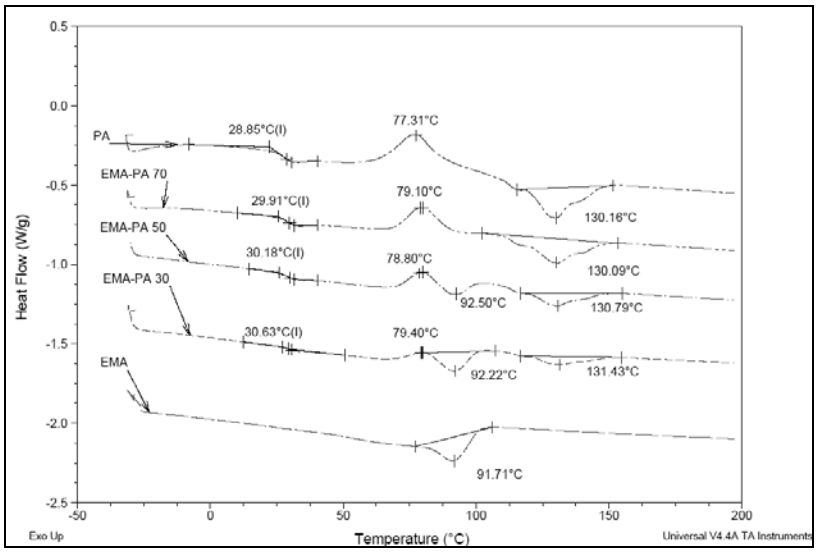

FIGURE 1. DSC DIAGRAM OF EMA/PA BLENDS.

Scanning Electron Microscopy (SEM)

SEM images of 12wt% Nisaplin incorporated EMA/PA blends are shown in figure 2 . Image A shows dry swollen capsules that did not rupture, probably due to the depth of about 150μm and the distance between capsules. Furthermore, the capsule's inner surface seems rough because of dried Nisaplin solution which contains sodium chloride. Image B, C and D shows droplet morphology and swollen capsules at varying depts. The inner surface of the swollen capsules seems smooth, compared with the rough droplet morphology, this is due to the peripheral tensile stress that osmotic pressure generates as a result of exposure to water. Image E shows a ruptured capsule, probably due to the proximity to the surface and a few swollen capsules are seen nearby.

These images indicate that an osmotic pressure driven release is the main Nisaplin release mechanism [17] [18].

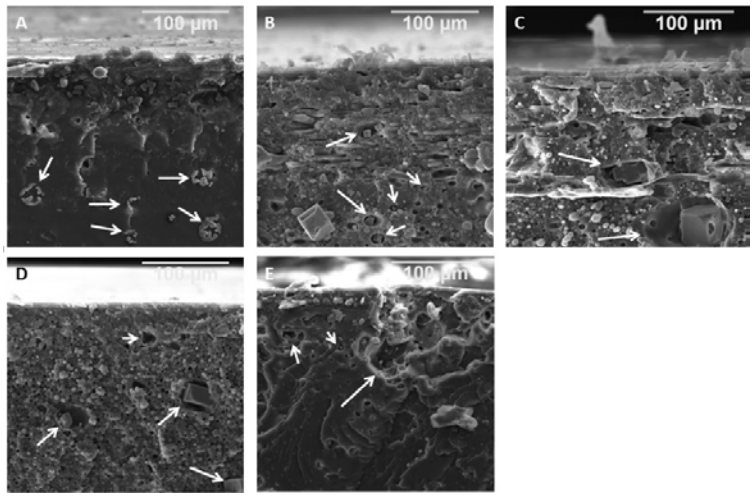

FIGURE 2. SEM IMIGES OF CROSS SECTION AREA OF: A: EMA/NIS12, B: EMA/PA-30/NIS12, C: EMA/PA-50/NIS12, EMA/PA-70/NIS12 AND E: PA/NIS12.

Nisin Migration Profile and Diffusion Coefficient Determination

Samples containing 12wt% of Nisaplin were characterized so that reliable data were obtained.

The migration profiles of samples that contain 4wt% of Nisaplin can be derived from 12wt% ones. This assumption can be made due to Nisaplin loading of 5.5vol% for 12wt% samples. This extent of loading is below the critical volumetric loading (about 33vol%) [17] [18]. Figure 3 illustrates plots of nisin concentration versus time for various matrix compositions. An initial steep raise of nisin concentration is seen within the first hour probably due to Nisaplin particles that are easily accessible to the simulant at the surface of the sample [19].

This steep raise is followed by some decrease, seen well in EMA/PA-30/Nis12 and EMA/PA-70/Nis12 samples. These samples may experience a tendency towards the influx of DI water containing nisin that was released in the first burst, rather than a balance or a tendency towards nisin migration, like EMA/PA-50/Nis12 and PA/Nis12.

It can be seen that different matrix compositions give different migration profiles with time. Furthermore, after 24 hours of exposure, the final concentration of different samples is spanned over a range of 2–6μg/ml that correspond to 0.6–2.0wt% of total nisin content released.

The corresponding diffusion coefficients, specified in table 2, were determined by the trend line slops of fractional release vs. square root of time plots (1-24 hours), figure 4, according to Fick's second law – equation 1 [20] [21]:

$$\frac{M_t}{M_\infty} = \frac{2}{L_p}\left(\frac{D \cdot t}{\pi}\right)^{0.5} \quad (1)$$

Where t is time [hours], $\frac{M_t}{M_\infty}$ is the fractional release at time t, D is the diffusion coefficient $\frac{m^2}{h}$ and L_p is the sample thickness m. It should be noted that equation 1 is valid for $\frac{M_t}{M_\infty} \leq 0.6$.

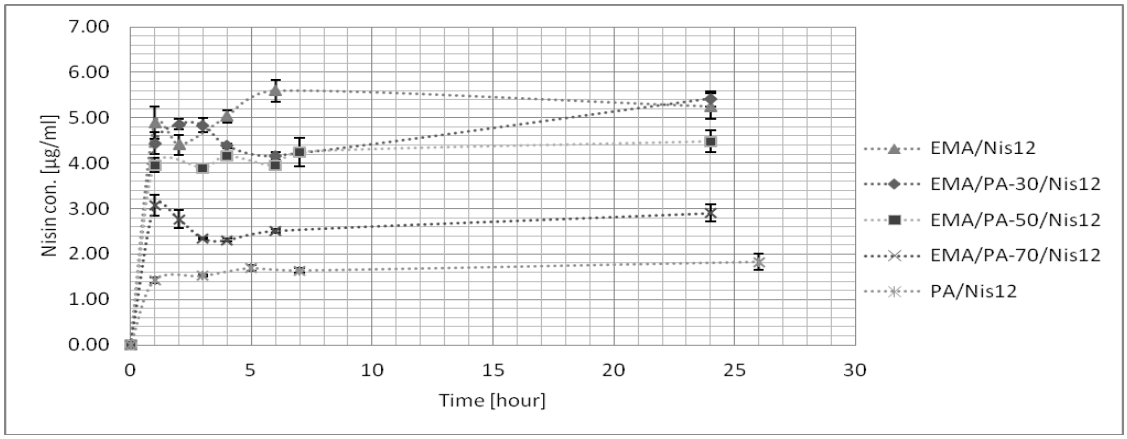

FIGURE 3. MIGRATION CURVES OF EMA/NIS12, EMA/PA-30/NIS12,EMA/PA-50/NIS12, EMA/PA-70/NIS12 AND PA/NIS12 AT 20°C. ERROR BARS REFER TO ±2Σ.

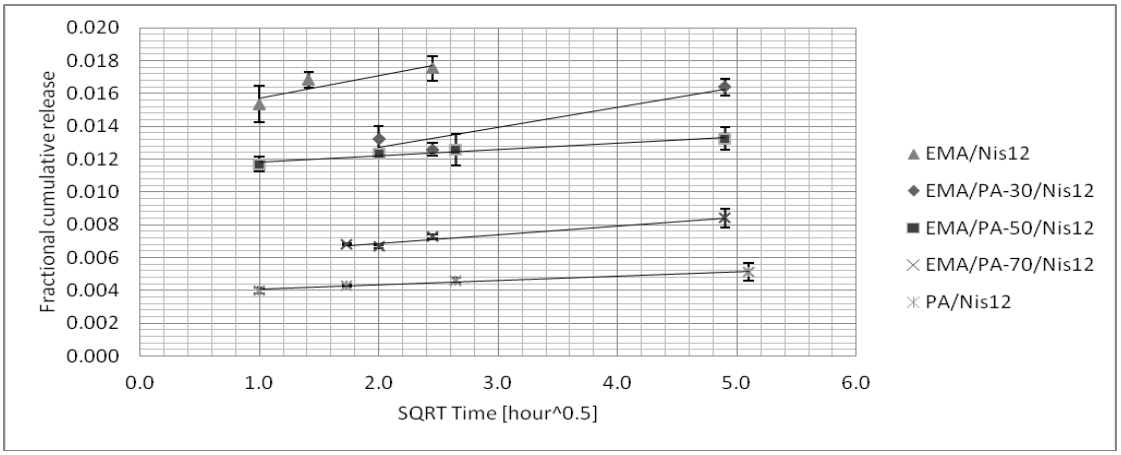

FIGURE 4. PLOTS OF FRACTIONAL RELEASE VERSUS SQARE ROOT OF TIME FOR THE MIGRATION OF NISIN FROM DIFFRENT POLYMER MATRIX BLEND COMPOSITIONS AT 20°C. ERROR BARS REFER TO ±2Σ.

TABLE 2. CALCULATED DIFFUSION COEFFICIENTS AND LEAST-SQUARES FIT FOR DIFFRENT POLYMER BLEND COMPOSITIONS.

Sample Notation	$D\left[\frac{m^2}{h}\right]$	R^2
EMA/Nis12	$2.12 \cdot 10^{-23}$	0.8123
EMA/PA-30/Nis12	$1.81 \cdot 10^{-13}$	0.9076
EMA/PA-50/Nis12	$2.01 \cdot 10^{-14}$	0.9663
EMA/PA-70/Nis12	$3.14 \cdot 10^{-14}$	0.9624
PA/Nis12	$1.13 \cdot 10^{-14}$	0.9777

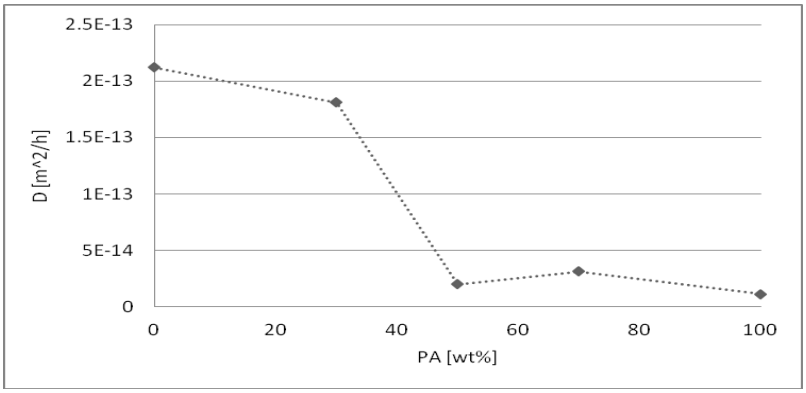

FIGURE 5. DIFFUSION COEFFICIANT AS A FUNCTION OF PA[WT%].

Figure 5 illustrates the change in the diffusion coefficients as a function of weight percent of PA in the polymer blend matrix. The diffusion coefficient decreases slightly when 30wt% of PA are introduced to neat EMA matrix. Considering further addition of PA, it can be seen that a sharp decrease is seen and further addition has no significant effect. SEM images reveal that droplet morphology exists differing in the inversion of component's role (figure 2). It is concluded that the diffusion coefficient is governed by the continuous phase.

All samples, except EMA/Nis12, have a least square fit above 0.90 and that diffusion is the dominant release mechanism. EMA/Nis12sample has a lower least square fit (0.81). This can indicate that diffusion is not the only release mechanism in action at this case.

Mechanical Properties

Samples consisting of neat EMA/PA polymer blends were characterized in order to evaluate the influence of the mechanical properties on the migration extent.

Figure 6 illustrates nisin concentration post migration of 24 hours to deionized water (data from figure 3) and elastic modulus as a function of PA content (numerical values are listed in table 3).

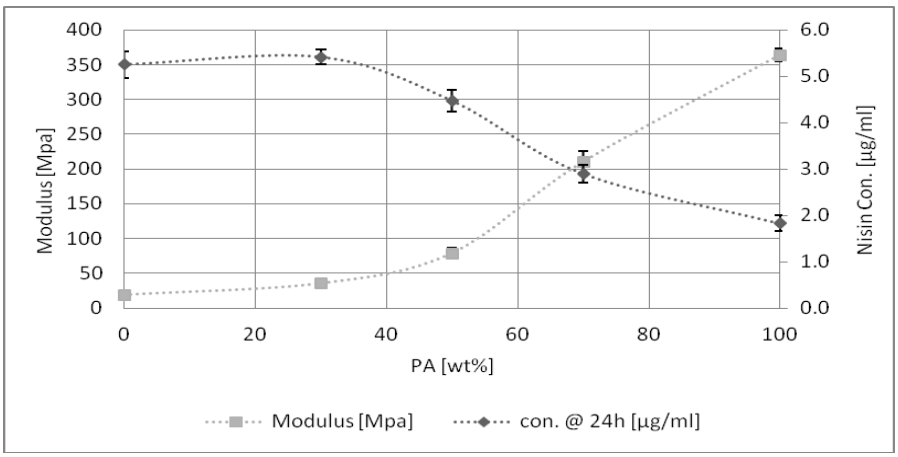

FIGURE 6. ELESTIC MODULUS AND NISIN CONCENTRATION AFTER 24 HOURS OF IMMERSION AS A FUNCTION OF PA[WT%]. ERROR BARS REFER TO ±2Σ.

TABLE 3. CORRESPONDING NUMERICAL VALUES FOR FIGURE 6.

PA[wt%]	Nisin Concentration [μg/ml]	Modulus [Mpa]
0	5.3±0.3	19±1
30	5.4±0.2	35±2
50	4.5±0.2	79±8
70	2.9±0.2	210±15
100	1.8±0.2	364±9

It can be seen that an inverse proportion exists. This inverse proportion can be related to the swelling extent of Nisaplin capsules and by that, nisin migration extent. As the water front enters a capsule, an osmotic driven release mechanism takes place (discussed earlier). This mechanism induces tensile stress at the perimeter of the capsule and as a result the capsule strains. It is known that the elastic modulus is inversely proportional to strain. As the polymer matrix modulus decreases, more capsule strain occurs and more surface area of Nisaplin solution is exposed for migration.

Similar results were seen when different sizes of BSA and sodium chloride granules were incorporated into silicone rubber. Results show that larger granules produce higher release profiles. It can be understood that when the capsule's size is larger, more surface area is exposed for migration [22].

Similar results were shown when sodium iodide was incorporated into silicone rubber with varying grain size. It was concluded that coarser granules lead to faster salt release [23].

Antibacterial Activity

Antibacterial activity tests were done in order to evaluate target bacteria response to different nisin migration profiles. The antibacterial activity of the different films was evaluated after 24 hours of exposure to different films.

It can be seen from figure 1 that all active films reduced target bacterial count compared with the natural growth of target bacteria (control). These results indicate that films of EMA/Nis4 and EMA/PA-30/Nis4 reduce bacterial count 4 fold, film of EMA/PA-50/Nis4 reduce bacterial count 7 fold and film of EMA/PA-70/Nis4 and PA/Nis4 reduce bacterial count 1-2 fold. Concerning figure 3, EMA/PA-50/Nis4 migration profile shows a lower concentration profile with time compared with EMA/Nis4 sample. It is known that target bacteria are susceptible to specific migration profiles more than others. In this case, migration profiles were determined by the polymer matrix composition. This result is coherent with studies that dealt with inhibition significance of target bacteria exposure to different nisin migration profiles [9] [10].

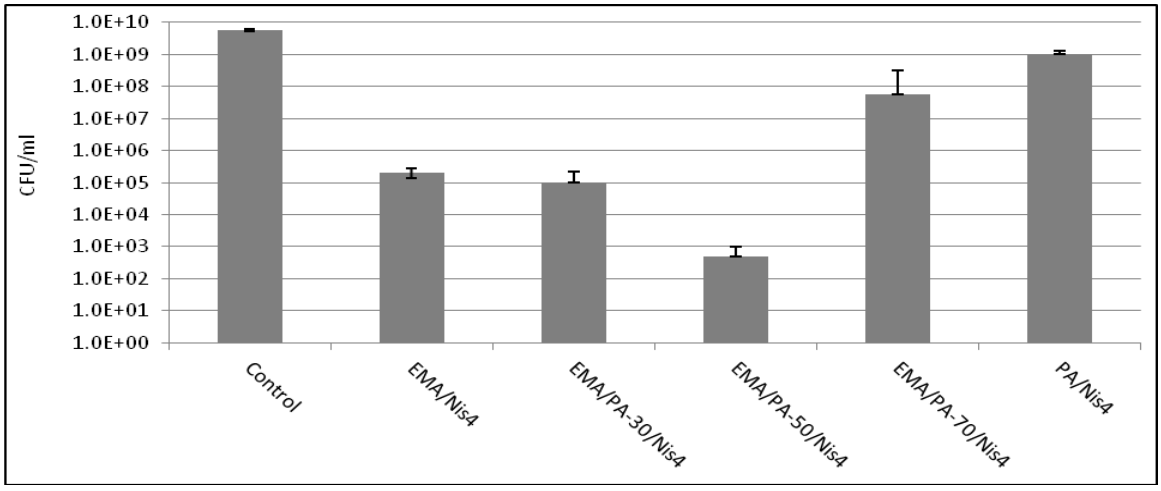

FIGURE 7. ANTIBACTERIAL ACTIVITY OF DIFFERENT SAMPLES. ERROR BARS REFER TO ±2Σ.

Conclusions

This study investigated different EMA/PA blends and its induced nisin migration profiles with the aim of enhancing the effectiveness of Nisaplin incorporated antibacterial active packaging. Nisin retained its antibacterial

activity when subjected to temperature of 160°C for 5.5 minutes.

The diffusion coefficient was mainly determined by the continues phase of the polymer blend matrix.

The use of an immiscible polymer blend, as different composition ratios , altered the matrix modulus. This induced different surface areas ready for migration. It is concluded that by controlling over the elastic modulus of the polymer matrix "fine tunes" the release profile, nisin incorporated active packaging effectiveness is enhenced. Antibacterial activity tests show that target bacteria response depends on nisin delivery profile.

Comparing these results with our previous study (EVA/PA blends incorporating Nisaplin), the migration profiles and diffusion coefficient induced are different at this case. This means that EMA has different influence on nisin release kinetics. This can be related to the relatively higher polarity that EMA contributes to EMA/PA blend than EVA dose for EVA/PA blend. Antibacterial activity tests show that the induced migration profiles in this study are more effective than the ones shown by EVA/PA blend. Higher antibacterial activity is seen at higher NB concentration.

Acknowledgments

The authors would like to thank The Israel Plastics & Rubber Center (IPRC) for funding this study; Michal Natan for helpful support regarding antibacterial activity tests; and AIT CHEMICALS for their cooperation regarding co-polyamide supply.

REFERENCES

[1] J. M. Lagaron, M. J. Ocio and A. Lopez-Rubio, Anitmicrobial polymers, Hoboken: John wiley & sons, 2012.

[2] S. Quintavalla, "Antimicrobial food packaging in the meat industry," Meat science, vol. 62, pp. 373-380, 2002.

[3] P. L. Dawson, "Effect of Lauric acid and Nisin-impregnated soy-based films on the growth of Listeria Monocytogens on turkey bologna," Poultry science, no. 81, pp. 721-726, 2002.

[4] J. H. Han, "Antimicrobial food packaging," Foodtechnology, vol. 54, no. 3, pp. 56-65, 2000.

[5] J. Eluned, V. Salin and G. W. Williams, "Nisin and the market for commercial bacteriocins," Department od agricultural economics, Texas, 2005.

[6] V. Coma, "Bioactive packaging technologies for extended shelf life of meat-based products," Meat science, vol. 78, pp. 90-103, 2008.

[7] J. Delves-Broughton, "Nisin and its application as a food preservative," Journal of the Society of Dairy Technology, vol. 43, no. 3, pp. 73-76, 1990.

[8] W. Liu and N. Hansen, "Some chemical and physical properties of nisin, a small-protein antibiotic produced by Lactococcus lactis," Applied and environmental microbiology, vol. 56, no. 8, pp. 2551-2558, 1990.

[9] Y. Chi-Zhang, "Effective control of Listeria monocytogenes by combination of nisin formulated and slowly released into a broth system," International journal of food microbiology, no. 90, pp. 15-22, 2004.

[10] Balasubramanian, "Effect of Nisin's controlled release on microbial growth as modeled for micrococcus luteus," Probiotics & Antimicro. Prot., no. 3, pp. 113-118, 2011.

[11] T. Jin, L. LinShu, Z. Howaed and H. Kevin, "Antimicrobial activity of nisin incorporated in pectin and polylactic acid composite films bagainst Listeria monocytogenes," International journal of food science and technology, vol. 44, pp. 322-329, 2009.

[12] S. Freiberg and X. X. Zhu, "Polymer microspheres for controlled drug release," International journal of pharmaceutics, vol. 282, pp. 1-18, 2004.

[13] L. Liu, "Antimicrobial Packaging Materials from Poly(Lactic Acid) Incorporated with Pectin-Nisaplin Microparticles," Chemistry and chemical technology, vol. 3, pp. 222-230, 2009.

[14] M. Gibaldi and S. Feldman, "Establishment of sink conditions in dissolution rate determinations," Journal of pharmaceutical sciences, pp. 1238-1242, 1967.

[15] H. Lee, D. S. An, H. J. Park and D. S. Lee, "Wide-spectrum antimicrobial packaging materials incorporating nisin and chitosan in the coating," Packaging technology and science, vol. 16, pp. 99-106, 2003.

[16] R. Chapanian and B. G. Amsden, "Osmotically driven protein release from photo-cross-linked elastomers of poly(trimethylene carbonate) and poly(trimethylene carbonate-co-D,L-lactide)," Eropean journal of pharmaceutics and biopharmaceutics, no. 74, pp. 172-183, 2010.

[17] Amsden, "A model for osmotic pressure driven release from cylinderical rubbery polymer matrices," Journal of controlled release, vol. 93, pp. 249-258, 2003.

[18] B. Amsden, "Review of osmotic pressure driven release of proteins from monolithic devices," J pharm pharmaceut sci, pp. 129-143, 2007.

[19] S. N. Dimitrios, S. Merope and K. G. Papadokostaki, "Comparative study of the release kinetics of osmotically active solutes from hydrophobic elastomeric matrices combined with the characterization of the depleted matrices," Journal of applied polymer science, vol. 113, pp. 936-949, 2009.

[20] Young-Min-Kim, "Properties of Nisin-incorporated polymer coating as antimicrobial packaging materials," Packaging technology and science, vol. 15, pp. 247-254, 2002.

[21] K. G. Papadokostaki, S. G. Amarantos and J. H. Petropoulos, "Kinetics of release of particulate solutes incorporated in celllulosic polymer matrices as a function of solute solubility and polymer swellability. II. highly soluable solute," Journal of applied polymer science, vol. 69, pp. 1275-1290, 1997.

[22] V. Carelli, G. Di Colo, C. Guerrini and E. Nannipieri, "Drug release from silicone elastomer through controlled polymer cracking: an extention to macromolecular drugs," International journal of pharmacetics, no. 50, pp. 181-188, 1989.

[23] R. schirrer, P. thepin and G. torres, "Water absorption, swelling, rupture and salt release in salt-silicone rubber compounds," Journal of materials science , no. 27, pp. 3424-3434, 1992.

Experimental Investigations on Thermal Analysis and Thermal Characterization of Al 6061-Sic-Gr Hybrid Metal Matrix Composites

S A Mohan Krishna[1, a], T N Shridhar[2, b], L Krishnamurthy[3, c]

[1]Department of Mechanical Engineering, Vidyavardhaka College of Engineering, Mysore-570002, Karnataka, India

[2]Dept. of Mechanical Engineering, The National Institute of Engineering, Mysore-570 008, Karnataka, India

[3]Dept. of Mechanical Engineering, The National Institute of Engineering, Mysore-570 008, Karnataka, India

[a]mohankrishnasa@vvce.ac.in; [b]tns_nie@yahoo.com; [c]kitty_nie@yahoo.co.in

Abstract

Metal matrix composites are regarded to be one of the most predominant classifications in composite materials. The thermal characterization of hybrid metal matrix composites has been increasingly important in a wide range of applications. The coefficient of thermal expansion, thermal conductivity, thermal diffusivity and specific heat capacity are the most important properties of Metal Matrix Composites (MMCs). Since nearly all Metal Matrix Composites are used in various temperature ranges, measurement of thermal properties of MMCs as a function of temperature is necessary in order to know the behaviour of the material. In this research paper, the evaluation of thermal conductivity, thermal diffusivity, thermal expansivity and thermal capacity has been accomplished for Al 6061, Silicon Carbide and Graphite hybrid metal matrix composites from room temperature to 300°C. Aluminium based composites reinforced with Silicon Carbide and Graphite particles have been prepared by stir casting technique. The thermal behaviour of hybrid composites with different percentage compositions of reinforcements has been investigated. The results have indicated that the thermal properties of the different compositions of hybrid MMCs vary by the addition of Graphite with Silicon Carbide and Al 6061. Few empirical models have been validated for the evaluation of thermal expansivity and thermal conductivity of hybrid composites.

Keywords

Thermal Characterization; Thermal Expansivity; Thermal Conductivity; Reinforcements; Thermal Capacity; Empirical Models and Validation

Introduction

Metal Matrix Composites are the innovative materials that possess unlimited opportunities for modern material science and development. These materials satisfy the desired conceptions, objectives and requisites of the designer. The reinforcement of metals can have many different objectives. The reinforcement of light metals will have abundant possibility of application in areas where weight reduction has first priority [1]. Metal Matrix Composites have greater advantage compared with other composites. These materials possess higher temperature, higher yield strength and yield modulus and can be strengthened by different thermal and mechanical treatments. Hybrid Metal Matrix Composites (HMMC) are regarded as one of the advanced materials that comprises of light weight, high specific strength, good wear resistance and low thermal expansivity. Hybrid MMCs are exceptional materials that are fabricated by reinforcements of at least two types of materials into a tough metal matrix. These hybrid composite materials are extensively used in structural, aerospace and automotive industries. Hybrid MMCs have greater relevance to automotive engineering concerning with piston rods, piston pins, braking systems, frames, valve spring caps, disk brake caliper, brake disks and disk pads [2].

Metal Matrix Composites have emerged as a category of productive materials for advanced structural, electrical, thermal management, electronic packaging and wear applications. MMCs exhibit noteworthy improvement in physical and mechanical properties compared with unreinforced Aluminium alloys. Aluminium is the most popular matrix for MMCs. Aluminium alloys are attractive due to their low density, their capability to be strengthened by precipitation, good corrosion resistance, high thermal and electrical conductivity and damping capacity. MMCs based on Aluminium alloys have received greater interest since they combine with low weight,

2226-4523/15/02 054-13 © 2015 DEStech Publications, Inc.
doi:10.12783/ijmsci.2015.0502.04

high mechanical strength, excellent wear properties, and are becoming potential as a material for many engineering applications [3].

Metal Matrix Composites have evoked a keen interest in recent scenario for potential applications in aerospace and automotive industries owing to their superior strength to weight ratio and high temperature resistance. The widespread adoption of particulate metal matrix composites for engineering applications has been hindered by the high cost of producing components. Although several technical challenges exist with casting technology, yet it can be used to overcome this problem. Achieving uniform distribution of reinforcement within the matrix is one such challenge, which affects directly on the properties and quality of composite material. In the present research, a modest attempt has been made to develop Aluminium matrix alloy with Silicon Carbide and Graphite reinforcements with an objective to accomplish thermal characterization of hybrid metal matrix composites [4, 5].

Metal Matrix Composites (MMCs) have been transformed from a topic of scientific and intellectual interest to a material of broad technological and commercial implication over the past few decades. There is an augmented demand for better materials in the area of dynamic structures, which demand high strength and light weight. Metal Matrix Composites assure to serve the intended purpose in this regard. They possess high toughness, excellent impact and fatigue strength, good thermal shock resistance, high thermal stability and high surface durability. There still exists the challenge and demand for developing metal matrix composites for use in high performance structural and functional applications including aerospace industries, automobile sector and defence. The objective of developing these composite materials is to agglomerate the desirable properties of metal and particulates. Metal Matrix Composites consist of at least two chemically and physically distinct phases, suitably distributed to provide properties not obtainable with either of the individual phases. For many researchers, MMCs is often equated with the term light metal matrix composites. Substantial progress in the development of MMCs has been achieved in decent decades, so that they could be introduced into the most imperative applications [5, 6].

Literature Survey

Thermal studies of composite materials are gaining greater impetus in the present scenario. This will help to understand the properties of materials as they change with temperature. It is often used as a term for the study of heat transfer through structures. The thermal analysis and characterization of hybrid MMC will depend on the factors that influence on the prominent thermo-physical properties presents a major challenge since they are sensitive to the type of reinforcement and method of manufacture. The knowledge of the thermo-physical properties has been compulsory for designing the effective heat transfer elements, heat sinks, heat shields and opto-electronic devices. The need for the thermal analysis of hybrid metal matrix composites should be comprehensively discussed. Most of the thermal studies are mainly concerned with Aluminium matrix composites, but minimum information is available on hybrid composites. The behaviour of hybrid composite materials is often sensitive to changes in temperature. This is mainly because, the response of the matrix to an applied load is temperature-dependent and changes in temperature can cause internal stresses to be set up as a result of differential thermal contraction and expansion of the constituents.

Though the research work pertaining to mechanical, tribological and fatigue behaviour of composites is effectively accomplished, since emphasis needs to be given to the work related to the measurement of prominent thermal parameters namely thermal conductivity, thermal diffusivity, thermal capacity and thermal expansivity. The main parameter considered in thermal analysis of metal matrix composites is thermal conductivity. The increase in thermal conductivity of composites will depend on strength and porosity, which finds this property in aerospace and automobile applications extensively. Thermal diffusivity is an important property for materials being used to determine the optimal work temperature in design applications referred under transient heat flow. It is the thermophysical property that determines the speed of heat propagation by conduction during changes in temperature with time. The heat propagation is faster for materials with high thermal diffusivity [3]. The assessment of thermal parameters will benefit to evaluate heat capacity, variation in the intensity of heat, heat diffusion and heat release rate. For aerospace and automotive applications, low CTE, moderate thermal conductivity, specific heat capacity and high electrical conductivity of the composites will enhance the efficiency in all perspectives. The techniques recommended for the experimental investigations of thermal conductivity and thermal diffusivity are laser flash apparatus, and determination of thermal expansivity requires dilatometer and specific heat capacity can be estimated using differential scanning calorimeter.

L C Davis and B E Artz. [7] in their research paper have explained that the thermal conductivity of metal matrix composites, which are potential electronic packaging materials, has been calculated using effective medium theory and finite element techniques. The thermal boundary resistance, which occurs at the interface between the metal and the included phase (typically ceramic particles), has a large effect for small particle sizes. It has been found that Silicon Carbide particles in Aluminium must have radii in excess of 10 μm to obtain the full benefit of the ceramic phase on the thermal conductivity.

S Cem Okumus et al. [8] in their paper have studied on thermal Expansion and thermal conductivity behaviours of Al/Si/SiC hybrid composites. Aluminium-Silicon based hybrid composites reinforced with silicon carbide and graphite particles has been prepared by liquid phase particle mixing and squeeze casting. The thermal expansion and thermal conductivity behaviours of hybrid composites with various graphite contents and different silicon carbide particle sizes (45 μm and 53 μm) has been investigated. Results have indicated that increasing the graphite content improved the dimensional stability, and there has been obvious variation between the thermal expansion behaviour of the 45 μm and the 53 μm silicon carbide reinforced composites.

Parker W J et al. [9] have explained the flash method of determining thermal diffusivity, heat capacity and thermal conductivity. A high-intensity short-duration light pulse is absorbed in the front surface of a thermally insulated specimen a few millimeters thick coated with camphor black, and the resulting temperature history of the rear surface has been measured by a thermocouple and recorded with an oscilloscope and camera. The thermal diffusivity has been determined by the shape of the temperature versus time curve at the rear surface, the heat capacity by the maximum temperature indicated by the thermocouple, and the thermal conductivity by the product of the heat capacity, thermal diffusivity and the density.

Na Chen et al. [10] have reviewed on metal matrix composites with high thermal conductivity for thermal management applications. The latest advances in manufacturing process, thermal properties and brazing technology of SiC/metal, carbon/metal and diamond/metal composites have been presented. Key factors controlling the thermo-physical properties have been discussed in detail.

S X Xu [11] has investigated the temperature profile and specific heat capacity in temperature modulated Differential Scanning Calorimeter with a low sample heat diffusivity. The paper explains about a specific numerical model that is used to analyze the effects of thermal diffusivity on temperature distribution inside the test sample and specific heat measurement by TMDSC. The sample test results are presented to demonstrate the effects of material thermal diffusivity.

N R Pradhan and H Duan [12] have examined the specific heat and effective thermal conductivity of composites containing single and multi-wall carbon nanotubes. The specific heat and effective thermal conductivity in anisotropic and randomly oriented multi-wall carbon nanotube (MWCNT) and randomly oriented single-wall carbon nanotube (SWCNT) composites from 300 K to 400 K has been studied. The specific heat of randomly oriented MWCNTs and SWCNTs exhibited similar behaviour to the specific heat of bulk graphite powder.

E Morintale and A Harabou [13] have described the use of heat flows from DSC curve for calculation of specific heat of the solid materials. On the basis of the second law of thermodynamics, they have established a procedure for calculating the specific heat of solid materials using heat flow in the sample studied, and the rate of heating of the sample.

B Karthikeyan et al. [14] have elucidated specific heat capacity measurement of Al/SiCP composites by Differential Scanning Calorimeter. Good thermal control systems have been considered for various materials applicable for spacecraft applications. Differential Scanning Calorimeter has been employed to determine the specific heat capacity of 7075 Al /SiCP composites.

R Arpon and E Louis [15] have analyzed that thermal expansion behaviour of Aluminium/SiC composites with bimodal particle distributions where it summarizes that the thermal response and the coefficient of thermal expansion (CTE) of Aluminium matrix composites having high volume fractions of SiC particulate have been investigated. The experimental results for composites with a single particle size indicate that the hysteresis in the thermal strain response curves is proportional to the square root of the particle surface area per unit volume of metal matrix, in agreement with current theories.

R A Saravanan and J Narciso [16] have investigated on thermal expansion behaviour of particulate metal matrix composites explains that Aluminium-matrix composites containing thermally oxidized SiC particles of controlled diameter ranging from 3 to 40 μm have been produced successfully by vacuum assisted high-pressure infiltration. Their thermal-expansion coefficients (CTEs) were measured between 25°C and 500°C with a high-precision thermal mechanical analyzer (TMA), and compared with the predictions of various theoretical models. The thermal-expansion behavior of the three-phase Al/SiC/SiO_2 composite shows no significant deviation from the predictions of elastic analysis, since the measured CTEs lie within the elastic bounds derived by Schapery's analysis.

Tran Nam et al. [17] have studied on effect of thermal cycling on the expansion behaviour of Al/SiC composites which is carried out where the coefficient of thermal expansion (CTE) and accumulated plastic strain of the pure aluminium matrix composite containing 50% SiC particles during thermal cycling (within temperature range 298–573 K) has been investigated.

Microstructural Analysis of Hybrid Metal Matrix Composies

Microstructural analysis of hybrid metal matrix composites has been carried out using Scanning Electron Microscope. The specimens have been polished and etched as per standard metallographic procedure. The microstructure of the hybrid composites has been carried out for Al 6061 and reinforcements namely Silicon Carbide and Graphite by varying the volume fraction. The microstructural analysis of the hybrid composites has been advantageous to study the morphology and presence of porosity. This helps to understand the distribution of reinforcements namely Silicon Carbide and Graphite with the matrix alloy Al 6061. It is accounted in the literature that the evaluation of the distribution of reinforcements and porosity is favourable to carry out thermal analysis and characterization of composites [8]. FIGURE 1, 2, 3, 4 and 5 show the micrographs of the different compositions of the hybrid MMCs.

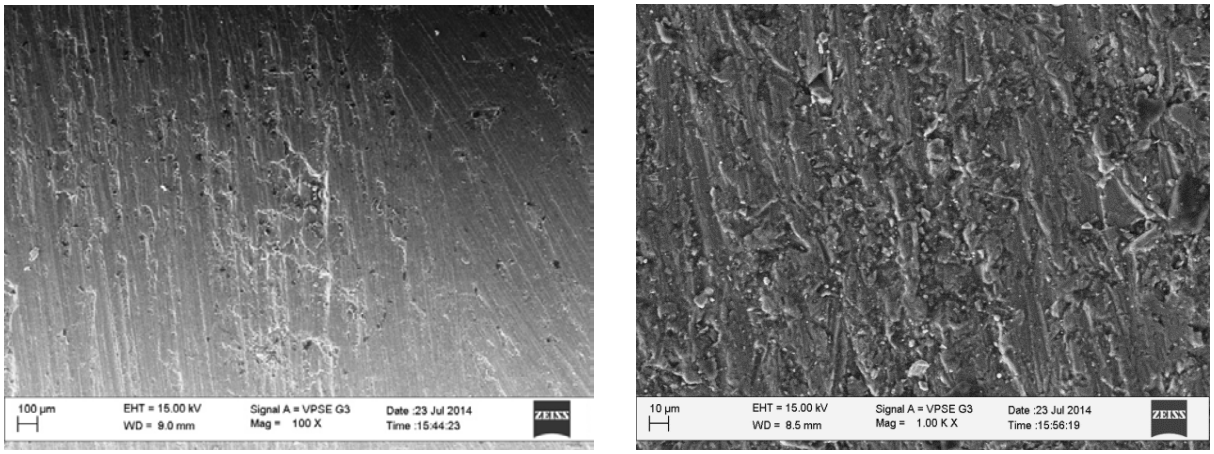

FIGURE 1. SEM MICROSTRUCTURES OF AL 6061 SAMPLE

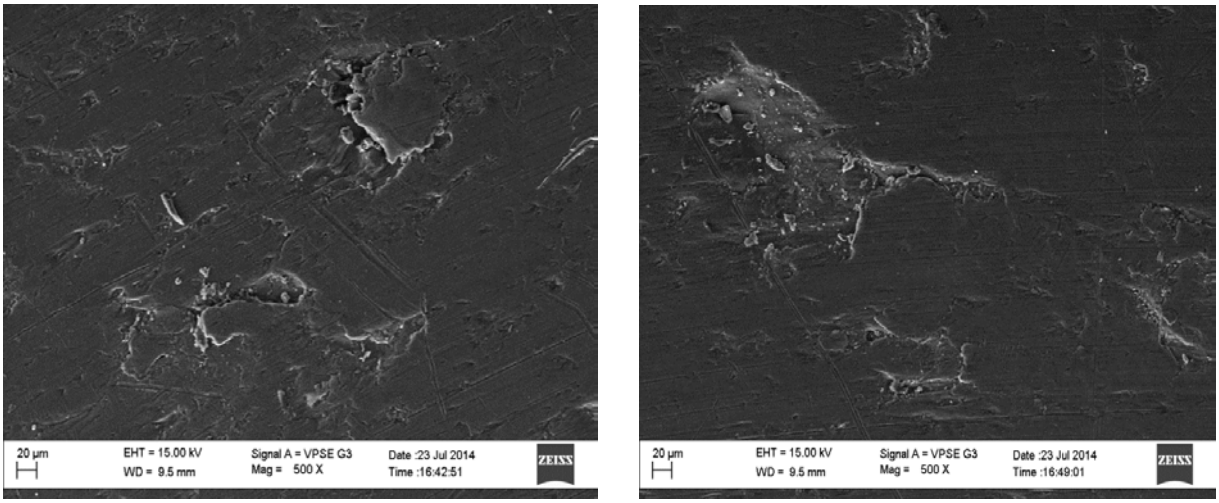

FIGURE 2. SEM MICROSTRUCTURES OF AL 6061 WITH 1.25% SILICON CARBIDE AND 1.25% GRAPHITE

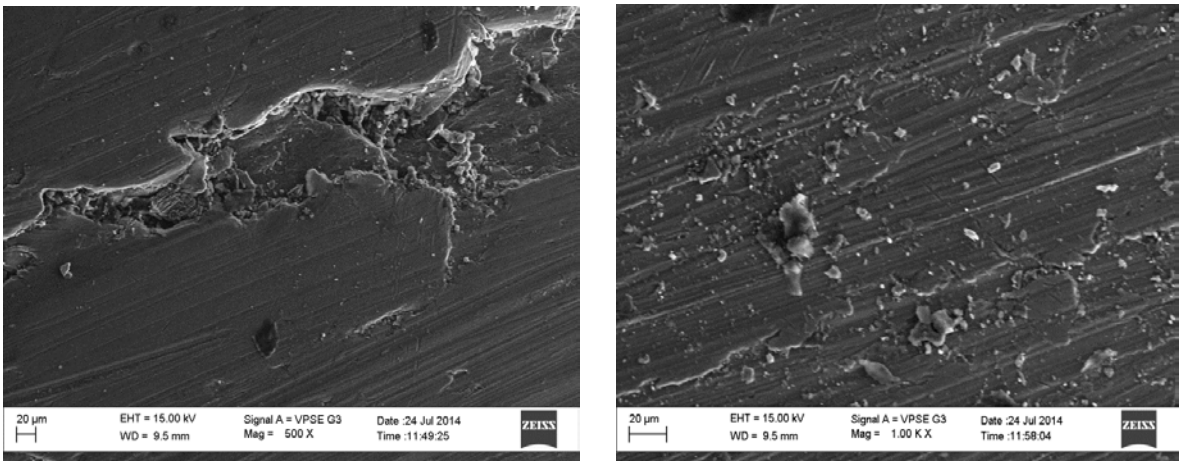

FIGURE 3. SEM MICROSTRUCTURES OF AL 6061 SAMPLE WITH 2.5% SILICON CARBIDE AND 2.5% GRAPHITE

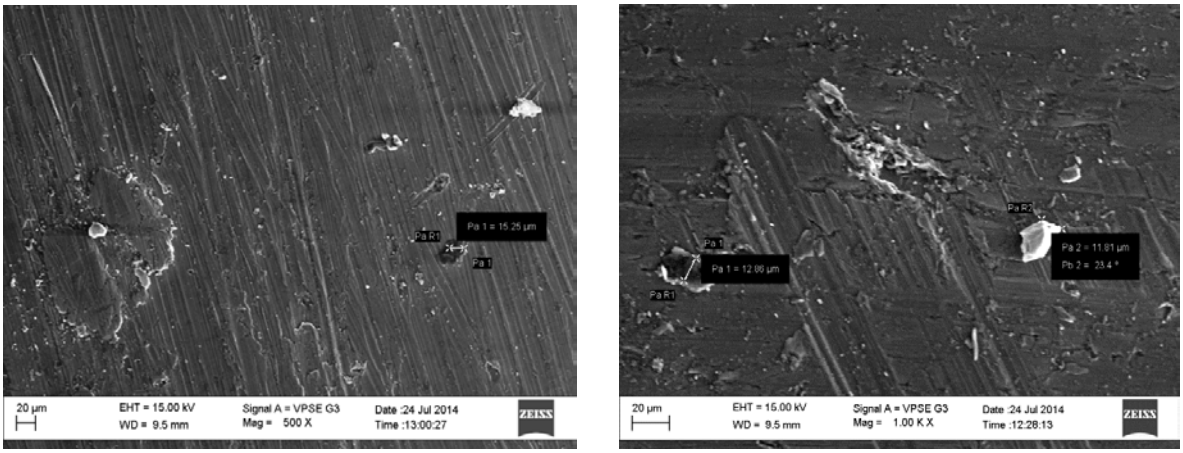

FIGURE 4. SEM MICROSTRUCTURES OF AL 6061 WITH 3.75% SILICON CARBIDE AND 3.75% GRAPHITE

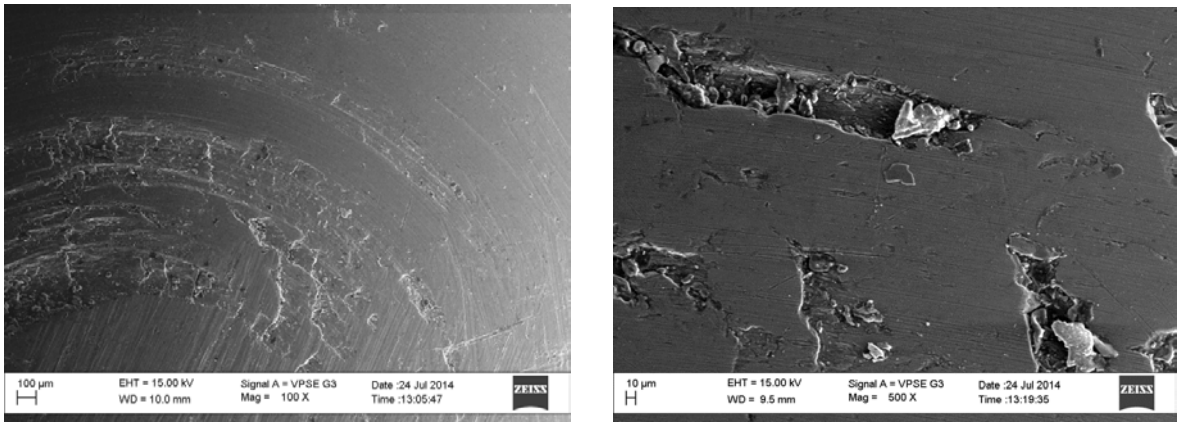

FIGURE 5. SEM MICROSTRUCTURES OF AL 6061 WITH 5% SILICON CARBIDE AND 5% GRAPHITE

FIGURE 1 depicts the micrographs of Al 6061 with no reinforcements. FIGURES 2, 3, 4 and 5 represent the micrographs of Al 6061 with the addition of reinforcements Silicon Carbide of varying weight fractions 1.25%, 2.5%, 3.75% and 5%. The dark patches indicate the presence of Graphite and white patchy layer specify the presence of Silicon Carbide. It can be observed that, with the addition of Silicon Carbide and Graphite with varying volume fraction, the distribution of the reinforcements is uniform with the absence of cracks and deleterious pores. Also, due to the variation in volume fraction of the reinforcements by performing constant stirring, the dispersoid concentration is uniform with minimum porosity. The porosity has been investigated both experimentally and theoretically. It has been reported in the literature that, increasing Graphite content in the composite matrix leads to grain refinement for Aluminium and eutectic Silicon and porosity. It has been stated that due to the increase in volume fraction of the reinforcements, the distribution is more reliable with negligible porosity. From the literature,

it has been investigated that, porosity can severely degrade the thermal and mechanical properties of MMCs [8, 14 and 17].

Experimental Investigation on Thermal Conductivity of Composites Using Laser Flash Apparatus

Laser Flash technique is highly resourceful for the evaluation of thermal conductivity and thermal diffusivity. The sample has been positioned on an electronically controlled and programmable robot located in a furnace. The furnace is then held at a predetermined temperature. At this temperature, the sample surface is then irradiated with a programmed energy pulse (laser or xenon flash). This energy pulse results in a homogeneous temperature rise at the sample surface. The resulting temperature rise of the rear surface of the sample is measured by a high speed infrared detector and thermal diffusivity values are computed from the temperature rise versus time data. The resulting measuring signal computes the thermal diffusivity, and in most cases the specific heat (Cp) data. Both power and the pulse length can be easily adjusted by the software [9]. The thermal diffusivity has been measured using a NETZSCH model LFA 447 Nano Flash diffusivity apparatus.

For the determination of thermal conductivity and thermal diffusivity, the sample should be disc shaped and size is as per ASTM standard. 5 samples have been considered with different percentage compositions. Al 6061 is the base alloy and reinforcements Silicon Carbide and Graphite with different percentage compositions or weight fractions 1.25%, 2.5%, 3.75% and 5% which have been selected. All the specimens have been tested from room temperature to 300°C. This temperature range have been selected so as to include the entire usable range of the composites, without the formation of liquid phase in the matrix The sample has been measured using a standard sample holder (diameter of 12.7 mm and thickness 3 mm). The sample has been coated with graphite on the front and back surfaces in order to increase absorption of the flash light on the sample's front surface and to increase the emissivity on the sample's back surface.

FIGURE 6 depicts the variation of thermal conductivity and temperature for the different compositions of hybrid metal matrix composites. FIGURE 7 indicates the variation of thermal diffusivity and temperature for the different compositions of hybrid metal matrix composites. The different samples have been tested from room temperature to 300°C using laser flash apparatus. From figure 6, it has been observed that, Al 6061 exhibits maximum thermal conductivity with 168 W/m K. Generally, the thermal conductivity increases as the temperature increases significantly. It has been be noticed that with the addition of reinforcements Silicon Carbide and Graphite to Al 6061, there is reduction in the thermal conductivity at maximum temperature for the different percentage compositions of hybrid metal matrix composites. Addition of Graphite with Aluminium matrix alloy and Silicon Carbide with varying volume fraction resulted in the reduction in thermal conductivity of the hybrid metal matrix composites. It has been reported in the literature that the thermal conductivity for hybrid MMCs considerably increases by reinforcing Silicon Carbide over the different range of temperatures. It has been inferred that, the reinforcement of Graphite with Aluminium and Silicon Carbide does not enhance thermal conductivity and thermal diffusivity significantly. It has been examined that addition of Silicon Carbide and Graphite reinforcements with high volume fraction results in higher values of thermal capacity, thermal expansivity and thermal conductivity. This has proved that the addition of reinforcements Silicon Carbide and Graphite has insignificant influence on the increase of thermal conductivity. The result indicated that graphite content improved the dimensional stability, and there would be no variation in thermal behaviour of hybrid composites [8, 14 and 15]. Based on these investigations, it can be concluded that the thermal conductivity of hybrid composites reduces due to the enrichment of graphite content. It can be concluded that the composites with 5% Silicon Carbide and 5% Graphite reinforced with Al 6061 exhibited low thermal conductivity compared with those of other hybrid composites for a consistent level of porosity. From literature, Aluminium-Silicon Carbide composites are attractive with many outstanding features, including higher thermal conductivity, lower thermal expansivity and low density. With any Aluminium matrix alloys, the addition of Silicon Carbide will enhance thermal conductivity and flexural strength [18, 19].

It has been reported in the literature that the dependence of the overall thermal conductivity on the particle diameter for spherical particles of equal size was investigated with several predictions. The genuine reason for the decrease of the thermal conductivity values with decreasing grain size of the different compositions of Silicon

Carbide can be attributed to the interfacial properties between the Al matrix and SiC. It is obvious that decreasing the grain size results in a larger surface area between Al matrix and SiC. The interfacial reaction between Al matrix and SiC can reduce the thermal conductivity of the composites. The porosity can severely degrade the thermal and mechanical properties of MMCs, SiC and graphite particles are uniformly distributed in aluminium matrix and no considerable level of pores was observed in the present study when graphite was used as reinforcement. Thermal conductivity was found to decrease as the content of graphite and the temperature increase, since reinforcements have lower thermal conductivities and because increasing temperature diminishes thermal diffusivity. The decrease in thermal diffusivity dominates the temperature dependence of thermal conductivity in the high temperature region. The specific heat decreases strongly at temperatures below room temperature and dominates the temperature dependence of thermal conductivity [8, 17 and 20].

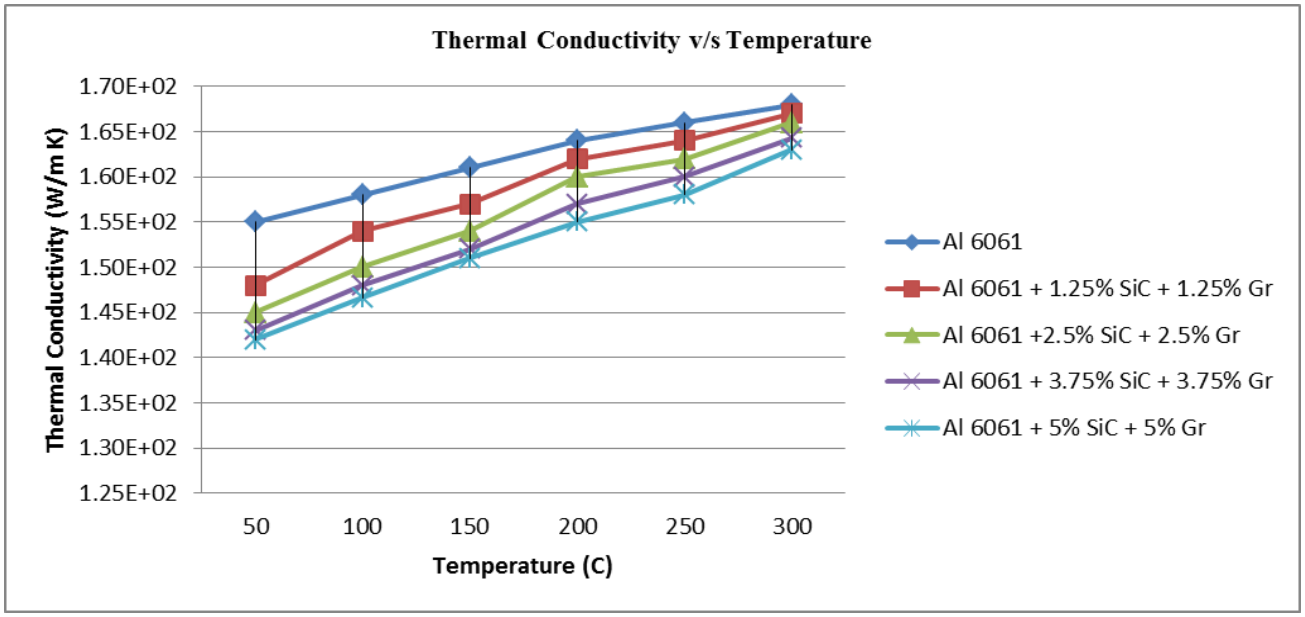

FIGURE 6. VARIATION OF THERMAL CONDUCTIVITY AND TEMPERATURE FOR DIFFERENT COMPOSITIONS OF MMCS

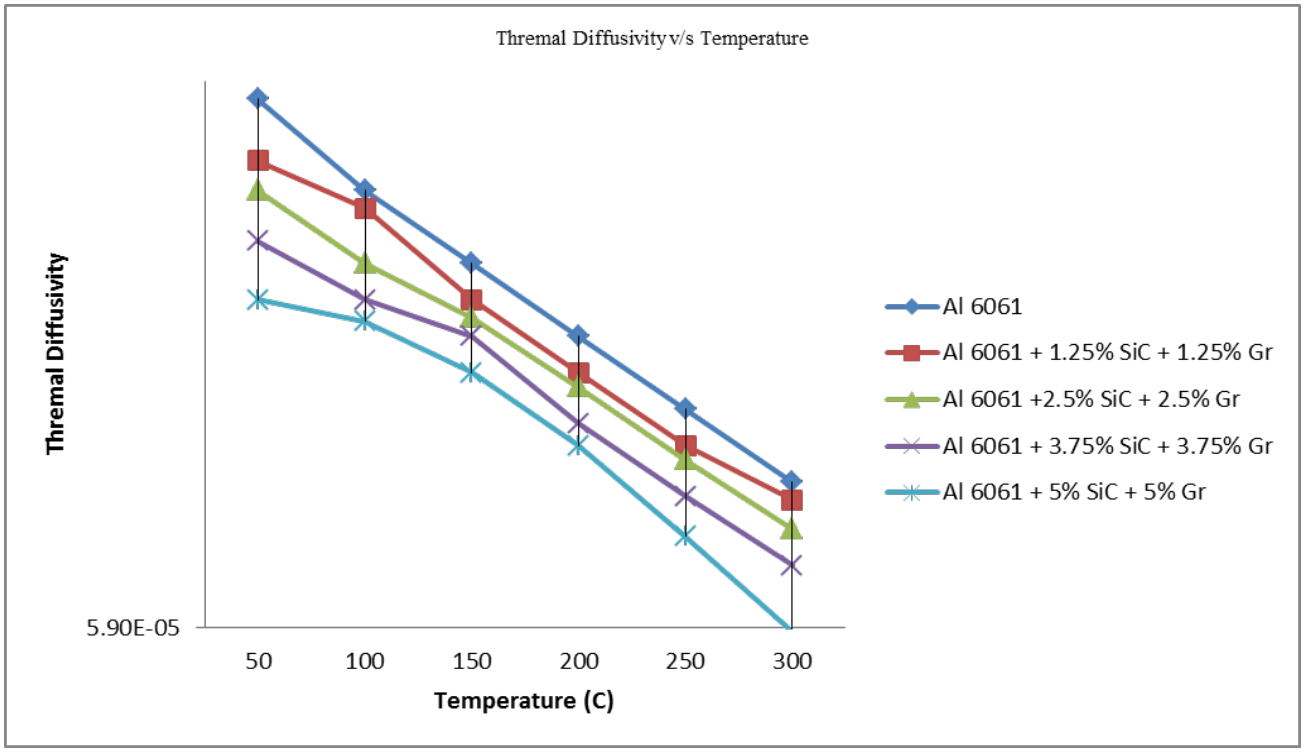

FIGURE 7. VARIATION OF THERMAL DIFFUSIVITY AND TEMPERATURE FOR DIFFERENT COMPOSITIONS OF MMCS

Mathermatical Validation of Thermal Conductivity Models

Theoretical prediction of effective thermal conductivity for multi-phase composite materials is very constructive for analysis and optimization of the material performance and for new material designs. The correct and accurate modelling for thermal coefficients of composite materials has a great value due to their excellent thermal and mechanical properties and their use in industrial applications and technological fields. The challenges in modelling complex materials come mainly from the inherent variety and randomness of their microstructures, and the coupling between the components of different phases. Several attempts have been made to develop expressions for effective thermal conductivity of two-phase materials by various researchers namely Maxwell, Lewis and Neilsen, Cunningham and Peddicord, Hadley, Rayleigh, Russel, Bruggemann,Meridith and Tobias, Hamilton and Crosser, Cheng and Vechon and Torquato. Numerical models have been developed over the last century to predict the thermal conductivity of two-phase composites for which dispersion of a second phase in a continuous medium of the first phase is assumed. The models have been applied to solid-gas or solid-solid composite systems.

In the present research, some of the empirical models considered in the evaluation of thermal conductivity are series model, Maxwell model, Geometric mean model, Russell model and Rayleigh model. FIGURE 8 represents the comparison of experimental values of thermal conductivity at maximum temperature with the mathematical models. The experimental values of thermal conductivity of different compositions of hybrid metal matrix composites are compared with various mathematical models. FIGURE 8 clearly indicates that the experimental values of thermal conductivity with varying volume fraction of composites closely match with series model, Maxwell and Rayleigh models, whereas the values deviate with reference to geometric model. It can be inferred that experimental data are in good argument with series model, Maxwell and Rayleigh models, but deviated from Geometric model.

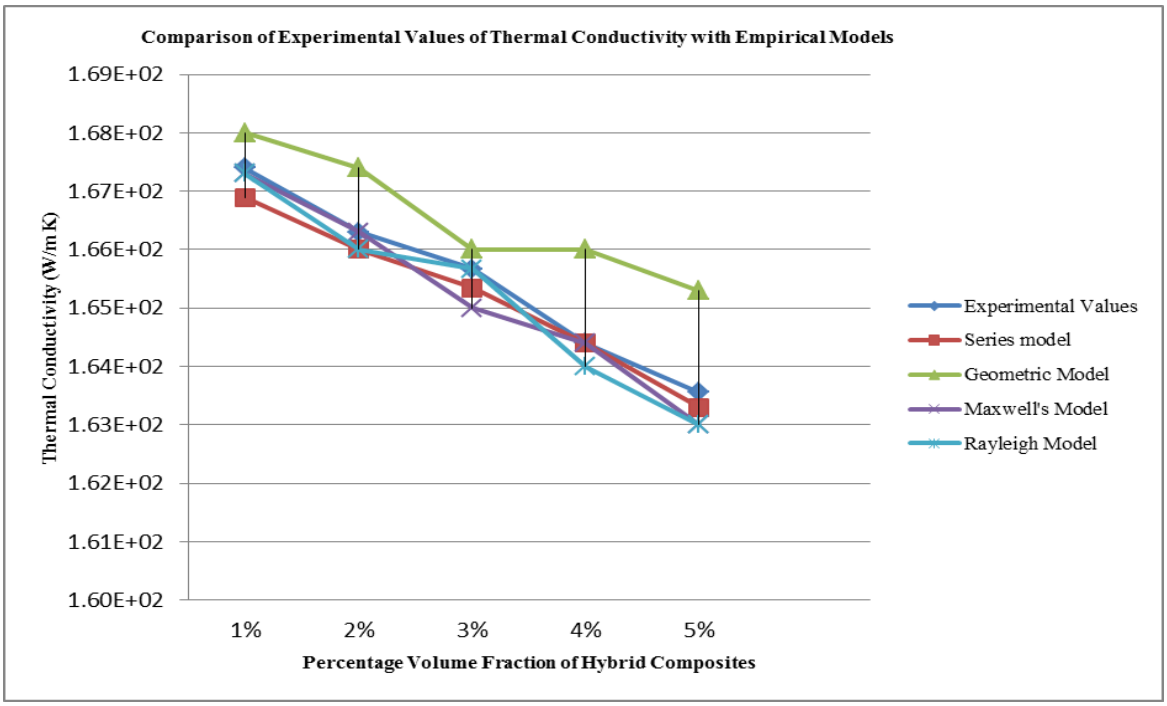

FIGURE 8. COMPARISON OF EXPERIMENTAL VALUES OF THERMAL CONDUCTIVITY WITH EMPIRICAL MODELS

Experimental Investigation on Coefficient of Thermal Expansion Using Dilatometer

In the research work, the coefficient of thermal expansion is determined using Linesis 75 Platinum Horizontal Dilatometer. Thermal expansion is the tendency of matter to change in volume in response to change in temperature. The degree of expansion to the change in temperature is called the material's coefficient of thermal expansion and generally varies with temperature. Coefficient of Thermal Expansion is one of the most important properties of MMCs. Since nearly all Metal Matrix Composites has been used in various temperature ranges, measurement of CTE as a function of temperature is necessary in order to know the behaviour of the material.

Several different systems for measurement of CTE can be used depending on the temperature conditions. One of the most common systems used is a dilatometer. A dilatometer measures the length or the volume changes of the sample, when the sample follows a temperature program and submits a small force. In a push rod dilatometer, the change in length of the sample is detected by an inductive displacement transducer. Calibration and corrections of measurements are done by using various standards and comparison with materials of known expansion.

For the determination of CTE, the size of the cylindrical sample is diameter 5 mm and length 10 mm. 5 samples are considered with different percentage compositions. Al 6061 is the base alloy and reinforcements Silicon Carbide (SiC) and Graphite (Gr) with different percentage compositions 1.25%, 2.5%, 3.75% and 5% which are selected. All the specimens have been tested from room temperature to 300°C. This temperature range has been selected so as to include the entire usable range of the composites, without the formation of liquid phase in the matrix. The data has been obtained in the form of per cent linear change versus temperature. Standard data analysis software was used to evaluate the Coefficient of Thermal Expansion (CTE) of the composites tested and was determined at intervals of 20°C. Rate Controlled Sintering (RCS) is an asset for standard dilatometer software. During measurement using dilatometer, the change in length of the sample for the required temperature range is considered. The purpose of RCS is to determine the optimal sinter process, especially the optimal temperature-time profile. Some of the salient parameters considered during the determination of CTE are sample length, relative density of the samples and sintering temperature. The melting point of Aluminium is 560°C. But during the testing process, it is limited to 300°C, as there is greater possibility of reaching molten condition.

FIGURE 9 depicts the variation of CTE and temperature for different compositions of hybrid MMC. It has been noticed that the CTE of the hybrid composites with different percentage compositions increases with the increase in temperature. From fig 9, it has been observed that Al 6061 exhibits maximum thermal expansivity. Generally, the thermal expansivity increases as the temperature increases significantly. It has been be noticed that with the addition of reinforcements Silicon Carbide and Graphite to Al 6061, there has been reduction in the thermal expansivity at maximum temperature for the different percentage compositions of hybrid metal matrix composites. Addition of Graphite with Aluminium matrix alloy and Silicon Carbide with varying volume fraction resulted in the reduction in thermal expansivity of the hybrid metal matrix composites. It has been reported in the literature that the thermal expansivity for hybrid MMCs considerably increases by reinforcing Silicon Carbide over the different range of temperatures [13]. It has been inferred that the reinforcement of Graphite with Aluminium and Silicon Carbide does not enhance thermal expansivity, thermal conductivity and thermal diffusivity significantly [14, 15]. It has been examined that addition of Silicon Carbide and Graphite reinforcements with high volume fraction results in higher values of thermal capacity, thermal expansivity and thermal conductivity.

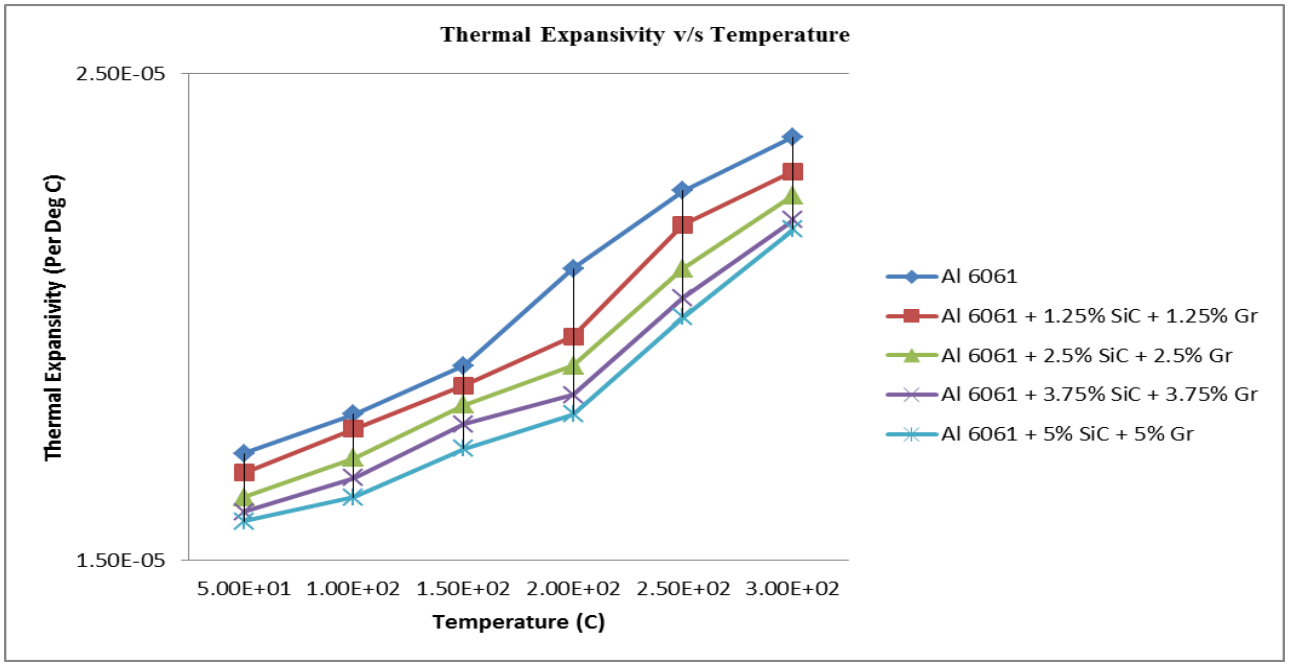

FIGURE 9. VARIATION OF CTE V/S TEMPERATURE FOR DIFFERENT COMPOSITIONS OF HYBRID COMPOSITES

Mathematical Validation of Empirical Models for the Evaluation of Coefficient of Thermal Expansion

The correct and accurate modelling for thermal coefficients of composite materials has a great value due to their excellent thermal and mechanical properties and their use in industrial applications and technological fields. The challenges in modelling complex materials come mainly from the inherent variety and randomness of their microstructures, and the coupling between the components of different phases. Several attempts have been made to develop expressions for thermal expansivity by various researchers namely Turner, Kerner, Schapery and Hashin-Shtrikman. Numerical models have been developed over the last century to predict the thermal expansivity and thermal conductivity of two-phase composites for which dispersion of a second phase in a continuous medium of the first phase is assumed. The models either assume or require as input a specific dispersion of second phase, and these have been reviewed by number of researchers.

To understand the thermal expansion behaviour of the hybrid composites, several existing theoretical models of composites are compared. When the interfaces are free to slide and the constituent phases are free to flow, the CTEs of the composites can be expressed by Rule of Mixtures. For a composite with perfect interfacial bonding between particles and matrix, Kerner's model is suitable for predicting the CTEs of composites. In Turner's model, each component of a composite undergoes a homogeneous strain throughout the composite [16, 19, 21 and 22]. In the present research, some of the empirical models considered in the evaluation of thermal expansivity are Rule of Mixtures, Kerner's model and Schapery's model. FIGURE 10 represents the comparison of experimental values of thermal expansivity at maximum temperature with the mathematical models. FIGURE 10 clearly indicates that the experimental values of thermal expansivity with varying weight fraction of composites closely match with Rule of Mixtures, Kerner's model and Schapery's model. It can be inferred that experimental data are in good argument with all mathematical models. It has been observed that, Rule of Mixtures exhibited the highest CTE, whereas Kerner and Schapery models exhibited lower values of CTE. It can be clearly inferred that Rule of Mixtures can be adjudged as the best empirical model for the evolution of CTE.

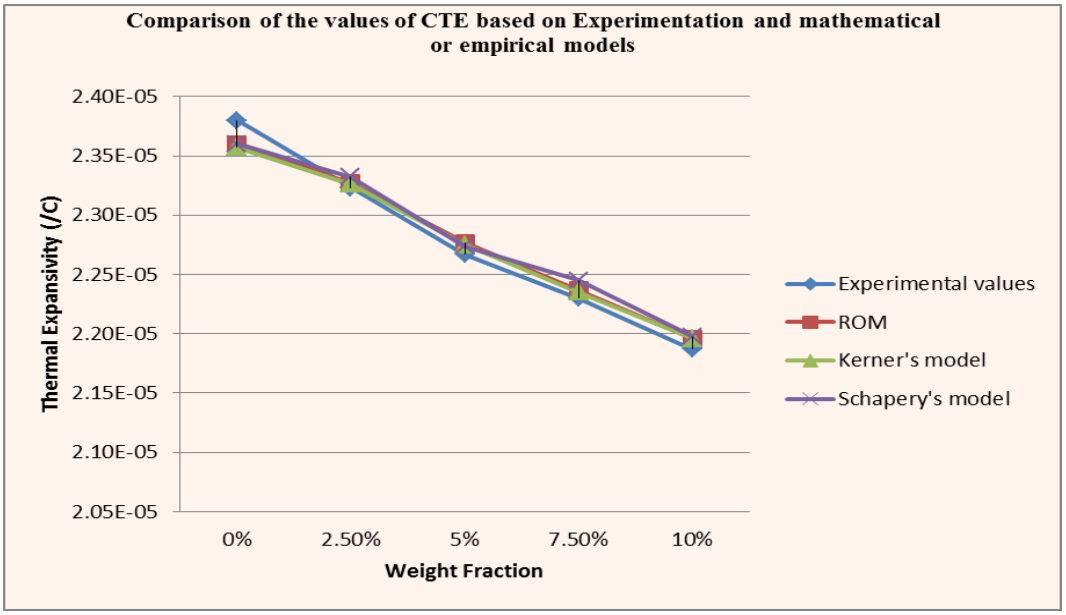

FIGURE 10. COMPARISON OF THE VALUES OF CTE BASED ON EXPERIMENTATION AND EMPIRICAL MODELS

Experimental Investigation on Specific Heat Capacity Using Differential Scanning Calorimeter

The technique recommended for the experimental investigation of heat flow distribution, specific heat capacity and enthalpy of hybrid metal matrix composites is Differential Scanning Calorimeter (DSC). DSC is one of the versatile thermal analysis techniques employed for measuring the energy necessary to establish a nearly zero temperature difference between a substance and an inert reference material, as two specimens are subjected to identical temperature regimes in an environment heated or cooled at a controlled rate. It can be used with composites and

composite precursors to study thermodynamic processes and kinetic events such as cure and enthalpic relaxation associated with physical aging or stress [11]. Differential Scanning Calorimeter (DSC) is one of the most periodically used techniques in the field of thermal characterization of solids and liquids. Its main advantages are the modest requirements in terms of sample size (~20 mg) and its ability to provide quantitative data on overall reaction kinetics, with relative speed and ease. Fundamentally, the DSC measures the heat capacity of a sample by recording the heat flow rate into the sample and comparing it with a reference sample.

In the present research work, the type of DSC proposed is heat flux for the determination of heat flow distribution and specific heat capacity. The experimentation has been carried out with DSC Q 200 F3 Maia, on a number of samples to measure specific heat functions. All samples have been encapsulated in the Aluminum foil dishes supplied with the instrument, which weigh approximately 20 mg with their covers. For the determination of Specific Heat Capacity and Enthalpy, the sample should be in powder form of about 20 mg. 5 samples have been considered with different percentage compositions. Al 6061 is the base alloy and reinforcements SiC and Graphite with different percentage compositions 1.25%, 2.5%, 3.75% and 5% which are selected. All the specimens have been tested from room temperature to 300°C. This temperature range has been selected so as to include the entire usable range of the composites, without the formation of liquid phase in the matrix

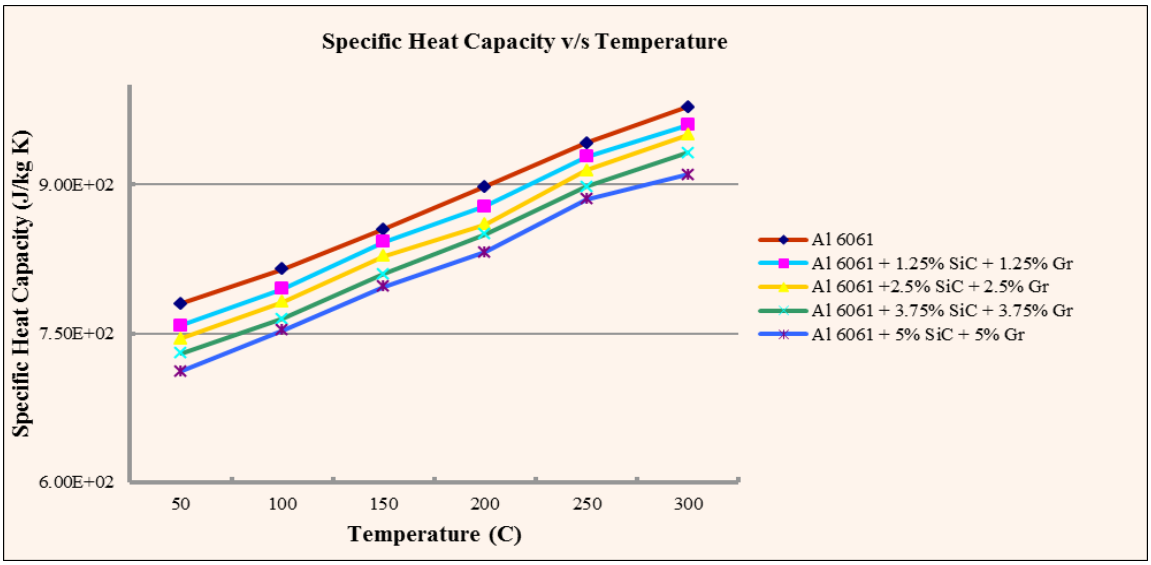

FIGURE 11. VARIATION OF SPECIFIC HEAT CAPACITY V/S TEMPERATURE FOR DIFFERENT PERCENTAGE COMPOSITIONS OF HYBRID COMPOSITES

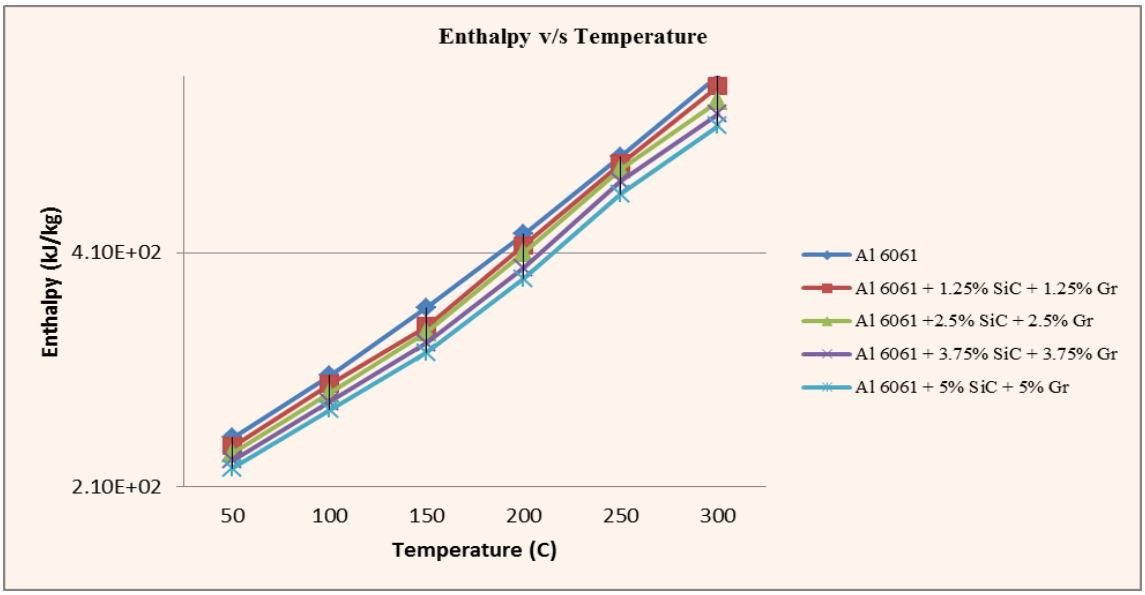

FIGURE 12. VARIATION OF ENTHALPY V/S TEMPERATURE FOR DIFFERENT PERCENTAGE COMPOSITIONS OF HYBRID COMPOSITES

The experimental investigation using DSC indicates the measurement of specific heat capacity over the range of temperatures. FIGURE 11 describes the variation of specific heat capacity and temperature for the different compositions of hybrid metal matrix composites. FIGURE 12 interprets the variation of enthalpy and temperature for the different compositions of hybrid metal matrix composites. Generally, the specific heat capacity increases as the temperature increases significantly. From FIGURE 11 and 12, it can be observed that Al 6061 exhibited maximum specific heat capacity and enthalpy with 980 J/kg K and 560 kJ/kg respectively. It can be noticed that with the addition of reinforcements Silicon Carbide and Graphite to Al 6061, there is reduction in the specific heat capacity and enthalpy at maximum temperature for the different percentage compositions of hybrid metal matrix composites. Addition of Graphite with Aluminium matrix alloy and Silicon Carbide with varying volume fraction resulted in the reduction in specific heat capacity of the hybrid metal matrix composites. It is reported in the literature that the specific heat capacity for hybrid MMCs considerably increases by reinforcing Silicon Carbide over the different range of temperatures [11]. From the literature, it can be inferred that the reinforcement of Graphite with Aluminium and Silicon Carbide does not enhance specific heat capacity significantly. It has been examined that addition of Silicon Carbide and Graphite reinforcements with high volume fraction results in higher values of thermal capacity, thermal expansivity and thermal conductivity [12]. The review based on the literature proves that the addition of Silicon Carbide and Graphite has insignificant influence in the increase of specific heat capacity. The result indicated that graphite content improves the dimensional stability, and there is no variation in thermal behaviour of hybrid composites [14]. Based on these investigations, it can be concluded that the specific heat capacity of hybrid composites reduces due to the enrichment of graphite content.

Conclusions

1. Al 6061 exhibits maximum value of thermal conductivity, thermal capacity and thermal expansivity, whereas there is a decline in all thermal properties of the hybrid composites at maximum temperature for the different percentage compositions of hybrid metal matrix composites with the addition of reinforcements Silicon Carbide and Graphite to Al 6061.
2. The thermal conductivity, thermal expansivity and thermal capacity of hybrid composites reduce due to the enhancement of graphite content.
3. The values of thermal conductivity, thermal expansivity and specific heat capacity decreas over the range of temperatures, with variation in density, variation in volume fraction of SiC and porosity of hybrid composites.
4. With the addition of reinforcements of low volume fraction or weight fraction, thermal conductivity, thermal expansivity and specific heat capacity of hybrid composites have been observed to be low.
5. The variation in thermal conductivity, thermal expansivity and thermal capacity depends on porosity, temperature variation, volume fraction, internal structure of the composites, dispersoid concentration of reinforcements and density of composites.
6. It has been inferred that experimental data are in good argument with series model, Maxwell and Rayleigh models, but deviated geometric empirical model.
7. It has been observed that Rule of Mixtures exhibited the highest CTE whereas Kerner and Schapery models exhibited lower value of CTE.

ACKNOWLEDGEMENTS

The authors wish to thank the prestigious company National Aerospace Laboratories, Bangalore for providing Horizontal Platinum Dilatometer facility to carry out the experimental work. The authors are extremely grateful to National Physical Laboratory, New Delhi and NETZSCH Technologies, Chennai for providing Differential Scanning Calorimeter and Laser Flash apparatus. They are indebted to Vignana Bhavan, University of Mysore, for helping to carry out microstructural analysis using Scanning Electron Microscope. They wish to thank the prestigious Visveshvaraya Technological University, Belagavi, Karnataka for the constant support and encouragement.

REFERENCES

[1] "Introduction to composites", Composites ASM Hand Book, Vol. 21, May 2002.

[2] N R Habbu "Use of Aluminium Silicon Alloys in Automobile Application", Proceedings of one day Industry Institute Interactive Meet on Al-Si alloys, Development and Application for transport sector, IISC Bangalore, September 2000.

[3] Karl Ulrich Kainer, "Basics of Metal Matrix Composites."

[4] Cory A Smith, DWA, "Discontinuous Reinforcements for Metal – Matrix Composites" Aluminium Composites, Vol. 121, Composites ASM International ASM Hand Book.

[5] Rajeshkumar Gangaram Bhandage and Parashuram Sonawane, "Preparation of Aluminium Matrix Composites using Stir Casting Method", International Journal of Engineering and Advanced Technology, ISSN: 2249-8958, Vol. 3, Issue 2, 2013.

[6] Ashish Srivastava, Prayag Garg, Yamini Krishna, "A Review on Fabrication and Characterization of Hybrid Metal Matrix Composites", International Journal of Advance Research and Innovation, Vol. 1, 2014, pp. 242 – 246.

[7] L C Davis and B E Artz, "Thermal Conductivity of metal matrix composites", Journal of Applied Physics, Vol. 77, 2009, pp. 4954-4960.

[8] S Cem Okumus, Sredar Aslan, Deniz Gultekin, Hatem Akbulat and Ramazan Karslioglu, "Thermal Expansion and Thermal Conductivity Behaviors of Al-Si/SiC/graphite Hybrid Metal Matrix Composites (MMCs)", Vol. 18, No. 4, 2012.

[9] Parker W J, Jenkins R J and Abbott G L, "Flash method of determining Thermal Diffusivity, Heat Capacity and Thermal Conductivity", Journal of Applied Physics, Vol. 31, Issue 9.

[10] Na Chen and Zhang, "Effect of Thermal cycling on the expansion behaviour of Al/SiC composites," Journal of Materials Processing Technology, 2009, pp. 1471-1476

[11] S X Xu, "Study of temperature profile and specific heat capacity in temperature modulated DSC with a low sample heat diffusivity", Elsevier, 2000, pp. 131-140.

[12] N R Pradhan and H Duan,"The specific heat and effective thermal conductivity of composites containing single and multi wall carbon nanotubes", IOP Publishing, USA, May 2009.

[13] E Morintale and A Harabou, "Use of heat flows from DSC curve for calculation of specific heat of the solid materials", Physics AUC, Vol. 23, 2013, pp. 89-94.

[14] B Karthikeyan, S Ramanathan and V Ramakrishnan, "Specific Heat Capacity of Al/SiC particles by Differential Scanning Calorimeter", Advanced Materials Research, Vol. 264-265, 2011, pp. 669-694.

[15] R Arpon and E Louis, "Thermal expansion behaviour of aluminium/SiC composites with bimodal particle distributions", Vol. 51, Issue 11, 2003, pp. 3145-3156.

[16] R A Saravanan and, J Narciso, "Thermal expansion studies on aluminium-matrix composites with different reinforcement architecture of SiC particles" Vol. 51, Issue 11, 2003, pp. 3145-3156.

[17] Tran Nam and, Requena, "Thermal expansion behaviour of aluminium matrix composites with densely packed SiC particles", Applied Science and manufacturing, Part A 39, 2009, pp. 856-865,.

[18] N Chawla and X Deng, "Thermal expansion anisotropy in extruded SiC particle reinforced 2080 aluminium alloy matrix composites", Material Science and Engineering A, 426, 2006, pp. 314-322.

[19] Lee H S and Hong S H, "Pressure Infiltration Casting Process and Thermophysical Properties of High Volume Fraction Al/SiC Particles Metal Matrix Composites, Materials Science and Technology 19(8), 2003, pp. 1057-1064.

[20] Antonyraj Arockiaswamy, R M German, Wang, Suri and Park, "DSC analysis of Al 6061 aluminium alloy powder by rapid solidification", Journal of Thermal Analysis and Calorimetry, 2010, pp. 361-366.

[21] Zhang and Wu, "Microstructure and thermal conduction properties of an Al-12 Si matrix composite reinforced with dual sized SiC particles", Journal of Materials Science, Vol. 39, 2004,pp. 303-305.

[22] Q Zhang, G Wu, G Chen, L Jiang and B Luan, "The Thermal Expansion and Mechanical Properties of High Reinforcement Content Al/SiC Composites Fabricated by Squeeze Casting Technology", Applied Sciences and Manufacturing, Elsevier, 2003, pp. 1023-1027.

High Porous Gamma-Alumina Synthesized by a Modified Sol-Gel Technique

Soledad Perez-Catán[1], M. Mónica Guraya[2,3*]

[1] Centro Atómico Bariloche, Comisión Nacional de Energía Atómica, Argentina

[2] Complejo Tecnológico Pilcaniyeu, Comisión Nacional de Energía Atómica, Argentina

[3] Extensión Áulica Bariloche, F.R.B.A., Universidad Tecnológica Nacional

*guraya@cab.cnea.gov.ar

Abstract

We prepared high porous γ-Al_2O_3 samples via a modified sol-gel method in which polyvinyl-alcohol (PVA) was incorporated to hydrolysis water before the formation of boehmite sol with two different PVA contents (44 and 174 wt%). We compared our results with those of other γ-Al_2O_3 samples also prepared via sol-gel with different procedures; a sample without additives (sample S) and samples with the same contents of PVA but added to the already synthesized boehmite sol (A-samples); the latter as standard for evaluation of our modified sol-gel method (B-samples).

Samples were characterized by means of XRD, adsorption-desorption isotherms of nitrogen at 77K and DTA-TG, and also were investigated against thermal cycling at 600 °C.

Pore volume, porosity, BET area, and pore distribution were determined. B-sample with 44 wt% PVA showed similar characteristics to those of A-samples, while an important increase of pore volume, porosity and BET area (50%) was observed for sample with 174% PVA. Pore diameter of B-samples also exhibited a different behaviour with PVA content: addition of 44 wt% of PVA gave a 16% increase while 174 wt% PVA, 42%. These results indicated that adding PVA to the already sinthesized boehmite sol, mainly stabilizes the boehmite structure, without affecting it. On the contrary, incorporation of PVA before hydrolysis influences the particle size in the sol, greatly modifying the final boehmite network and giving place to larger pores in the final γ-Al_2O_3, this effect being significant when adding 174 wt% PVA.

Results of thermal treatments at 600°C showed a decrease in BET area of all samples up to 80h, then stabilised. A minimal effect of the thermal treatments on the pore volume and porosity was observed in all samples while the pore diameter increased, this increase being most important in case of sample with 174 wt% PVA.

Keywords

Gamma-alumina; PVA Additives; Sol-gel

Introduction

Development of porous ceramics has been extensively investigated for years, due to its applicability in numerous chemical processes. The intrinsic properties of aluminium oxide, such as high melting point, low thermal conductivity, chemical inertness and corrosion resistance have made aluminas of use to many different industrial and technical processes [1-3]. Among these materials, γ- Al_2O_3 presents extraordinary properties as good thermal and chemical stability, high specific surface area and surface with proportion and distribution of chemical active centers. Sol-gel technique has proved particularly efficient in producing samples with such characteristics [4-6]. This technique consists in the hydrolysis of an aluminium alcoxide to a suspension that, after peptising, becomes a colloidal suspension or sol; by evaporation, this sol turns into gel and, after calcination, into a metal oxide [7]. The porous structure of the material derived from this method is highly dependent on the preparation and calcination parameters, and to the incorporation of additives [4-8].

Polyvinyl-alcohol (PVA) is a linear polymer, frequently used as a binder in conventional ceramic industry, which has been reported to improve the quality of thin films prepared by sol-gel methods [9]. In particular, several authors have studied the effect of addition of PVA to γ- Al_2O_3 coatings [10-12]; they reported that this polymer

2226-4523/15/02 033-7 © 2015 DEStech Publications, Inc.
doi:10.12783/ijmsci.2015.0502.01

reduced the stress in the film network and in the film-support interface. In addition, adequate adjustment of PVA content in boehmite sols and aging time were proved essential in avoiding cracking in the supported films.

Regarding the influence of PVA on the porous structure of γ- Al_2O_3, Ecsedi et al. have found that this additive favoured formation of macropores [13]. Haridas and Bellari studied gellability for aluminium alkoxides; their results showed a change in hydrolysis velocity when varying hydrolysis-pH [14]. Water content in gels and synthesis temperature can modified boehmite gel network, thus leading to different temperature values for the transition boehmite to γ-Al_2O_3, and therefore, to different porous structure in the calcined alumina [5, 15, 16].

PVA polymer forms its own gel matrix with higher drying temperature than boehmite network. For this reason, the PVA structure is more flexible to adapt itself to the boehmite matrix, during the drying of the latter. Cui et al, obtained nickel nanoparticles supported on gamma-alumina by incorporating an organic additive in order to control gelation velocity [17]. PVA additive was incorporated to boehmite sol, where solvated boehmite particles were already arranged in a fairly stable network.

The aim of this work was to prepare γ-Al_2O_3 samples with high surface area and microporous structure, stabile to cyclic thermal treatment, by means of a modified sol-gel method in which PVA additive was added to water before hydrolysis of the aluminium alkoxide, and also to study the influence of the amount of PVA on the sample porous structure.

Experimental

Samples of γ-Al_2O_3 were prepared by sol-gel process, following Yoldas technique [7] as a general procedure. The boehmite colloidal suspension was prepared by hydrolyzing an aluminium sec-butoxide, prepared in our laboratory, in a large excess of water (H_2O/Alkoxide=100 mol/mol) at 80-100°C, followed by peptization with mineral acid (HNO_3) ratio 0.08 mol/mol acid/alcoxide, to yield a stable particulate sol. Aqueous solution of 10% (P/P) Polyvinyl alcohol (M = 9000) was incorporated as additive to the boehmite sol in Method A and to water before hydrolysis of the aluminium alkoxide in our modified method (Method B). Two PVA contents, 44 and 174 wt% (PVA/alumina %), were included for both preparation methods. A γ-Al_2O_3 sample without additive was also prepared for comparison.

Gelation is generally achieved by concentration of the sol via boiling or evaporation but in our case was accelerated by PVA addition. Gels deposited in Petri dishes, were evaporated at 30°C, then dried at 100°C for 12 h and finally sintered at 600°C to eliminate PVA additive and transform boehmite to gamma-alumina.

Thermal treatments at 600°C in a stream of dry air were conducted for 12, 25, 50, 75, and 100h. Samples were named regarding the prepration method and the PVA content as A44 and A174, B44 and B174; sample S corresponds to the γ-Al_2O_3 sample prepared without additives.

The unsupported gamma-alumina samples were degassed to 450°C, 2h and then characterized by nitrogen adsorption-desorption isotherms at liquid nitrogen temperature (77K), in a Digisorb 2600 from Micromeritics Int. Corp. We used for the evaluation the model based on straight, non-interconnected cylindrical pores closed off at one end. Additionally, the algorithm used on the equipment is based on Faass's implementation of the B.J.H. method. Differential Thermal Analysis-Thermogra-vimetry (DTA-TG) experiments were carried out in a Netzsch STA 409 set-up in 60 cc/min dry air flow.

Powder X-ray Diffraction (XRD) measure-ments ($10° < 2\Theta < 90°$) were conducted in a Philips PW1700 diffractometer with Cu-K_α radiation and a graphite monochromator.

Results and Discussion

XRD spectra of the dried gels confirmed the formation of boehmite as can be seen in Figure 1. PVA spectrum is also shown, thus helping identification of the peak at 20° as belonging to PVA pattern. This peak appeared in spectra from samples with 174 wt% of PVA and was more intense in case of sample prepared by method B.

To investigate the influence of the preparation method on the boehmite to gamma-alumina transition, DTA–TG experiments were carried out for samples with 44 wt% of PVA by both Methods A and B as well as for sample

prepared without additive. The results are shown in Figure 2. Four temperature regions have been defined according to mass losses detected by DTG: region I, up to 200°C, region II from 200 to 340°C, region III from 340 to 650°C, and region IV for temperatures higher than 650°C. The mass loss observed in region I is associated to water desorption for all samples. Region II shows a DTG endothermic peak due to desorption-decomposition of residual organics. Different features can be observed in region III depending on the sample. In this temperature range two processes occurred: endothermic transition from boehmite to γ-Al_2O_3 and PVA exothermic combustion.

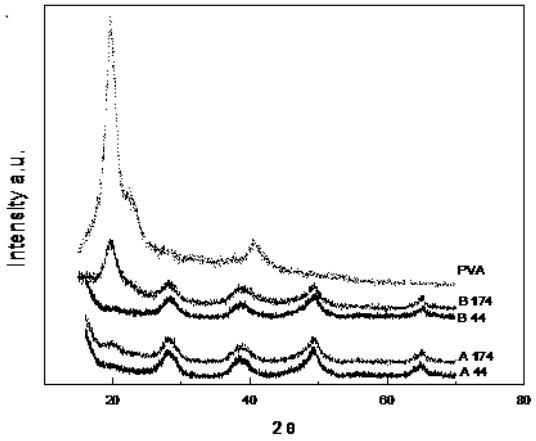

FIGURE 1. XRD SPECTRA FROM DRIED GELS OF SAMPLES PREPARED WITH 44 WT% PVA.

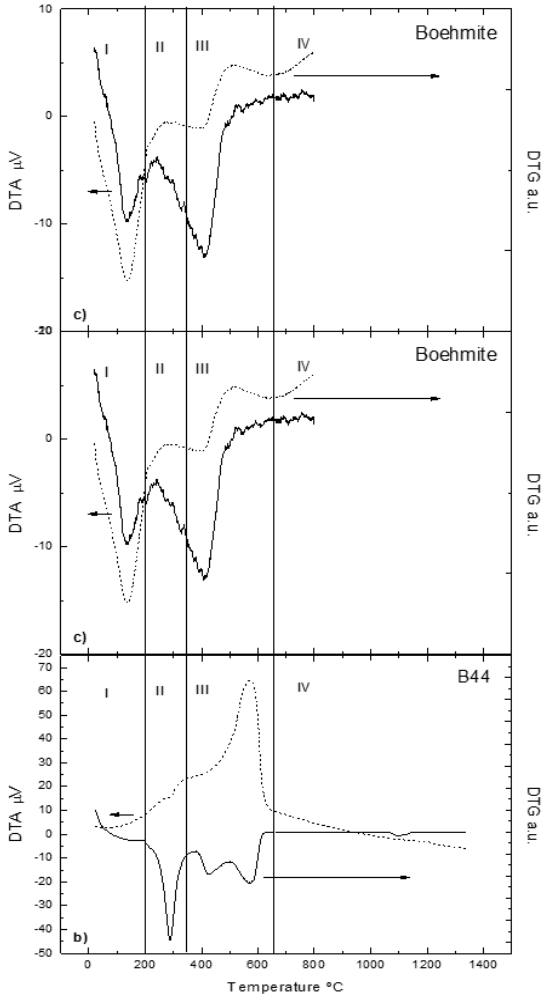

FIGURE 2. DTA-DTG FROM DRIED GELS OF SAMPLES A44 (A); B44 (B), AND S (C)

Two sharp structures can be distinguished in DTG curve from Figure 2b, at 430 and 570°C, which are associated to those processes. For sample A44 (Figure 2a), a broad DTG peak is observed, that can be assigned to both alumina

transition and PVA combustion, whose structures appear so close in temperature that cannot be resolved; in DTA curve however, these endo- and exothermic processes can be distinguished at 410 and 490°C, respectively. On the curve corresponding to sample S (Figure 2c) the transition boehmite to gamma-alumina was determined at 410°C.

After calcination at 600°C for 12h, XRD spectra (not shown) only indicated the presence of gamma-alumina in all samples. In order to analyse the thermal stability of the porous structure in time, temperature treatments at 600°C for different periods were conducted. From nitrogen adsorption experiments, BET areas, pore volumes, porosity, and volume pore distributions were determined. Results obtained for samples after 12h calcination and after 100h temperature treatment are presented in Table 1.

TABLE 1. POROUS STRUCTURE PARAMETERS DERIVED FROM NITROGEN ADSORPTION EXPERIMENTS FOR SAMPLES AFTER 12 H CALCINATION AT 600°C AND AFTER 100 H TREATMENT AT 600°C.

	Treat-ment Time (h)	Sample				
		S	**A 44**	**A 174**	**B 44**	**B 174**
BET surface area (m^2/g)	12	245	320	286	332	368
	100	160	220	241	214	251
Pore Volume (cm^3/g)	12	0,26	0,39	0,44	0,39	0,66
	100	0,24	0,40	0,50	0,37	0,63
Porosity (%)	12	43	60	62	60	72
	100	48	60	66	58	71
Mean pore diameter (Å)	12	38	38	44	38	55
	100	46	55	60	54	80

In the following, we will firstly discuss the porous structure of the calcined samples and, afterwards, the evolution of that structure with treatment time.

Regarding samples after calcination, volume pore distributions are shown in Figure 3. Samples A44 and B44 presented rather narrow pore distributions, centred at 40 Å, and very similar to that of the gamma-alumina prepared without additive. Increasing PVA content produced broader pore distributions, which shifted towards larger pore diameters; this effect was much more important in case of samples where PVA was incorporated to hydrolysis water.

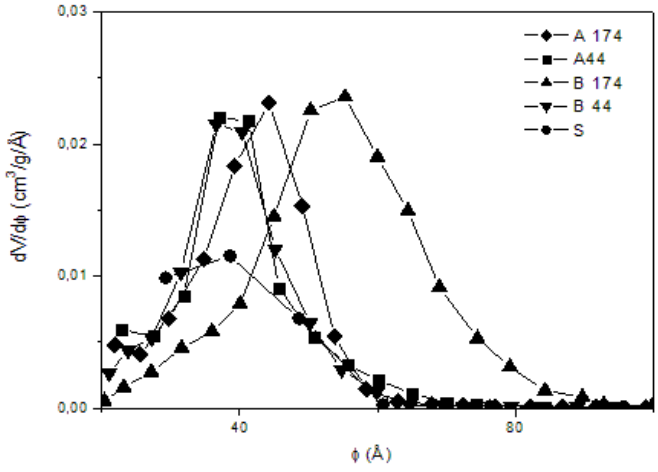

FIGURE 3. PORE SIZE DISTRIBUTION FOR SAMPLES AFTER 12H CALCINATION AT 600°C

In Table 2, with the purpose of simplifying the analysis, relative changes in structural parameters determined for A- and B- samples are presented. An "increasing" factor F% = (P_{PVA} - P_S)/ P_S*100 was defined for every property P; PVA and S subscripts refer to samples prepared with and without additive, respectively. These results evidenced that although the mean pore diameter and the pore volume increased, no decrease in porosity was determined in samples with PVA.

TABLE 2. FACTOR F% THAT REFLECTS CHANGES IN POROUS STRUCTURE PROPERTIES DUE TO THE INCORPORATION OF PVA IN SAMPLES CALCINED 12H AT 600°C

Property \ Sample	F(%)			
	A		B	
	44	**174**	**44**	**174**
Pore volume	50	69	50	153
Porosity	40	44	40	67
Mean pore diameter	0	0	16	42
BET area	31	17	36	50

Both preparation methods exhibited different behaviour regarding PVA content, however. Data from Table 2 shows that addition of 44wt% PVA produces a similar effect on the final mesoporous structure, independently of the addition procedure. Their BET area, porosity, and pore volume values are ~ 40% higher than those for sample S, prepared without PVA; on the other hand, samples with 44wt% PVA presented pore diameters comparable to that of sample S. This result indicated that boehmite particles formed during hydrolysis were very similar in the three samples, regardless the presence of PVA and the preparation stage at which additive was incorporated. The effect of this polymer on the boehmite matrix would be stabilising the sol and avoiding sintering during calcination, which probably is the reason for the high surface areas observed.

In general, incorporation of PVA to hydrolysis water favours the interaction between polymer and the boehmite particles, which are still forming. Ecsedi et al have demonstrated that increasing PVA content, modified texture in macro- and mesoporous alumina [12, 13]. As a consequence of polymer-boehmite interaction, gel network, gelation point, and therefore, alumina porous structure should be different from the structure obtained when adding PVA to the already formed boehmite sol. Similar results were found by Kim and co-workers, in relation to high thermal stability in sol-gel derived alumina [5]. Furthermore, boehmite particles or agglomerates synthesised in presence of this linear polymer are different in diameter, thus leading to also different porous structures as reported by Uhlhorn et al [11] and and also by Yang et al in the synthesis of Nd_2O_3 nanopowders [18]. The sample prepared by method B with substantial amount of PVA (174 wt%) seemed to respond to this model. This sample (Table 2) showed an important increase in pore diameter and, consequently, in pore volume with respect to the sample without additives. However, a higher porosity was also determined, thus giving as overall result an increase in the specific area.

This analysis is consistent with the results from sample A174; its BET area was higher than that of sample S prepared without additives but lower than the area from sample A44. PVA incorporated to boehmite sol would act as pore former, stabilise the sol network, and avoid formation of defects. Adding a great deal of polymer would produce larger pores, which might cause the decrease observed in BET area for sample A174.

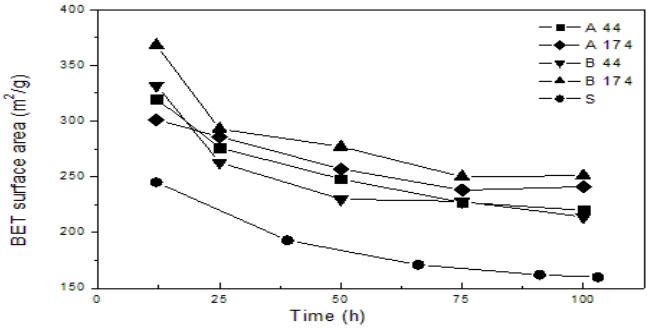

FIGURE 4. BET SURFACE AREA AS A FUNCTION OF TIME FOR SAMPLES TREATED AT 600°C.

The evolution of BET area with time on stream is shown in Figure 4, where rather parallel decreasing curves are observed for all samples; these curves seem to converge to a constant after 80h approximately. When increasing treatment time, some pore coalescence might be expected, that would increase pore volume and decrease specific area. This interpretation can explain the behaviour observed for all samples with and without PVA. The porous structure of A- and B-samples resulted as stable as the sample without additive; the improvement achieved by PVA addition persisted after 100h on stream.

The results from Table 1 showed that porosity and total pore volume in all samples were quite stable after 100h temperature treatments. On the other hand, a decrease in the specific area and an increase in the mean pore diameter were determined. Figure 5 shows the volume pore distribution of samples with 44 wt% PVA (a) and 174 wt% (b) after 100 h temperature treatment as compared to the corresponding calcined samples. After calcinations and 100h treatment S-sample results were also included for analyzing. The general effect of 100h treatment at 600°C in samples A44 and B44 was a shift of the distribution towards larger pore diameters. This behaviour was similar to that of sample S, which proved consistent with our previous discussion regarding samples after calcination.

In case of samples with 174 wt % PVA, the shift of pore distribution for A174 was a little higher (60 Å) while sample B174 showed the most important shift with final mean pore diameter at 80 Å; this sample showed as well the highest BET area after 100 h thermal treatment, 250 m^2/g. Although sample A174 also kept a high BET area after thermal treatment, its pore diameter and pore volume values were considerably lower than those from sample B174. All pore size distributions remained narrow as shown in Figure 5, with a full width at half maximum between 20 and 30Å. These results demonstrated the feasibility of preparing thermally stable samples with high porosity, high specific area, and large pores, which can be convenient for applying to coatings, where a different material provides mechanical support.

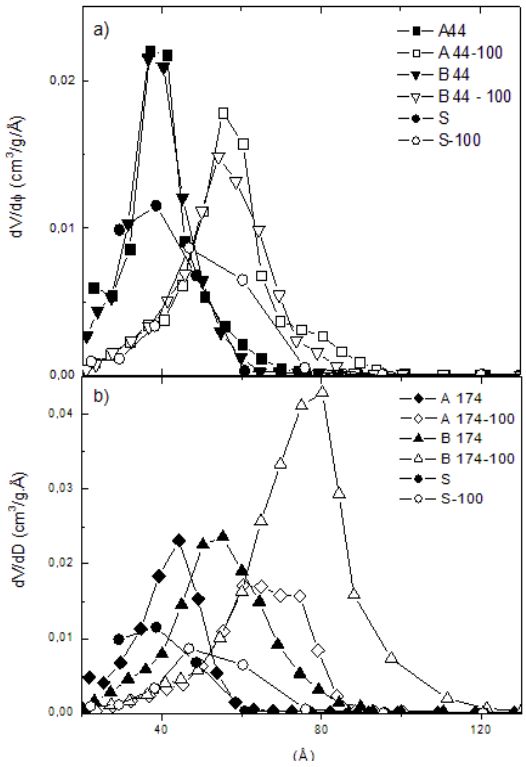

FIGURE 5. PORE SIZE DISTRIBUTION FOR SAMPLES AFTER 12H CALCINATION AND AFTER 100 H TREATMENT AT 600°C, PREPARED WITH (A) 44 WT% PVA AND (B) 174 WT% PVA.

In summary, our results showed that incorporation of PVA additive before hydrolysis gives place to an important modification of the porous structure of the final calcined samples, thus increasing BET area, pore diameter, pore volume and porosity. Substancial amounts of PVA produced samples that kept their properties after 100h of thermal treatment. Pore diameter values determined for these samples were higher with a narrow distribution.

Conclusions

The incorporation of PVA as an additive before hydrolysis of aluminium- secbutoxide (Method B) produced γ-Al_2O_3 samples with higher BET area, pore diameter, pore volume and porosity than those corresponding to addition of PVA to the bohemite sol (Method A).

Even though samples with specific area greater than 300m²/g were obtained by incorporation of PVA at the two different stages of boehmite synthesis, the highest BET area was achieved for the sample with 174 wt% PVA included in hydrolysis water.

Pore size distributions of samples prepared by Method A were very similar to that of sample S prepared without additives, with no change in the mean pore diameter value, thus indicating that PVA incorporated to boehmite sol would act as pore former and stabilise the sol network. On the other hand, samples prepared by Method B showed a shift of the whole distribution towards higher pore diameters, consistent with an important change in the boehmite structure and consequently producing much larger pores in the final gamma-alumina. This effect was moderate for 44 wt% content of PVA but important in case of adding 174 wt% of PVA solution. As the PVA was present during boehmite synthesis, the boehmite-sol particles were probably smaller, which would explain the higher pore volume and pore diameter, porosity, and BET area values obtained.

Porous structure of all samples proved to have narrow pore size distribution and showed a stable behaviour against thermal treatments up to 100 h at 600°C. Although a decrease in the BET area was observed for all samples, after ~80h on stream, curves stabilised at a constant value. Sample B174 showed the highest BET area after 100 h thermal treatment, 250m²/g as well as the highest pore volume and pore diameter.

γ-Al_2O_3 prepared by incorporation of substantial amounts of PVA to hydrolysis water merges as a good candidate for membrane coating applications.

ACKNOWLEDGMENT

The authors are very thankful to L. Dufou for carrying out the XRD analysis and G. Tejada and G. Pastrana for N_2 adsorption determinations. This work was partially supported by SCTyP from Universidad Nacional de Cuyo.

REFERENCES

[1] de Lange, R.S.A., K. Keizer , and A.J. Burggraaf, J. Membr. Sci. 104 (1995): 81-100.

[2] Haag, S., M. Burgard, and B. Ernst, Surf. Coat. Technol. 201 (2006): 2166-2173.

[3] Ahmeda, S., A. Aitani, F. Rahman, A. Al-Dawood, and F. Al-Muhaish, Appl. Catal., A 359 (2009): 1-24.

[4] Brinker, C.J. and G.W. Scherer, Sol-Gel Science, Springer, Berlin (1992).

[5] Kim, S., Y. Lee, K. Jun, J. Park, and H. Potdar, Mater. Chem. and Phys. 104 (2007): 56-61.

[6] Ferreira-Aparicio, P., I. Rodriguez-Ramos, and A. Guerrero-Ruiz, Appl. Catal., A. 237 (2002): 239-252.

[7] Yoldas, B., Am. Ceram. Soc. Bull., 54 (1975): 289-290.

[8] Jing, Chengbin, Xiujian Zhao, and Yongheng Zhang, Mater. Res. Bull. 42 (2007): 600-608.

[9] Zaspali, V.T., W. Van Pragg, K. Keizer, and J.R.H. Ross, J. Mater. Sci., 27 (1992): 1023-1035.

[10] Lin Y., and A.J. Burggraaf, J. Am. Ceram. Soc., 74(1991): 219-224.

[11] Uhlhorn, R.J.R., M.B.H.J. Huis, K. Keizer, and A.J. Burggraaf, J. Mater. Sci. 27 (1992): 527-537.

[12] Ecsedi, Z., I. Lazau, and C. Pacurariu, Appl. Ceram. 1 (2007): 5-9.

[13] Ecsedi, Z., I. Lazau, and C. Pacurariu, Microporous and Mesoporous Mater. 118 (2009): 453-457.

[14] Haridas M.M., and J.R. Bellare, Ceram. Intern., 25 (1999): 613-616.

[15] Guzmán-Castillo, M.L., F. Hernández-Beltrán, J.J. Fripiat, A. Rodriquez-Hernández, R. García de León, J. Navarrete-Bolaños, A. Tobón-Cervantes, and X. Bokhimi, Catal. Today 107–108 (2005): 874-878.

[16] Bokhimi, X., J. Sánchez-Valente, and F. Pedraza, J. Solid State Chem. 166 (2002): 182-190.

[17] Cui, H., M. Zayat, D. Levy, and Y. Zhang, J. Non Cryst. Solids 351 (2005): 2102-2106.

[18] Yang, W., Y. Qi, Y Ma, X. Li, X. Guo, J. Gao, and M. Chen, Mater. Chem. and Phys. 84 (2004): 52-57.